Solar Energy 276 (2024) 112687

Contents lists available at ScienceDirect

Solar Energy

journal homepage: www.elsevier.com/locate/solener

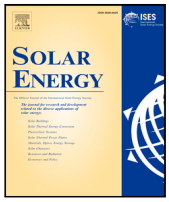

Investigating the annual performance of air-based collectors and novel bi-fluid based PV-thermal system

Zain Ul-Abdin *, Miro Zeman, Olindo Isabella, Rudi Santbergen

Photovoltaic Materials and Devices Group, Delft University of Technology, Mekelweg 4, Delft, 2628 CD, The Netherlands

ARTICLE INFO

Keywords:
Solar photovoltaic-thermal (PVT)
Air-based heating collectors
Bi-fluid heating collector
Modeling
Robust controller

ABSTRACT

This paper presents dynamic air-based models of a hybrid photovoltaic-thermal (PVT) collector. The models are developed with the aim of estimating the temperature of the collector components and therefore of estimating the annual generation of electrical energy and thermal energy outputs, by using actual climate data of six different cities based on Köppen-Geiger-Photovoltaic (KGPV) climate zones. The results show that the unglazed type collector has the best PV cooling while the dual channel collector has the best air heating among air-based PVT collectors. The results also indicate that the use of additional fluid enhances both electrical and thermal performance. The dynamic models are validated by comparison with results found in the literature. The paper also discusses a novel bi-fluid PVT system combined with a storage tank and an H-infinity based robust controller that can handle uncertainties. The results of the bi-fluid system show that the fraction of energy demand covered by the system is highly dependent on climate conditions and the collector's surface area. It was found that for a small-scale house (standard for four people), the proposed system can cover more than 70% annual domestic hot water demand for cities with high solar irradiance and 32% for a city with low solar irradiance.

1. Introduction

The rise in demand for sustainable energy solutions is on an upward trajectory and so does the utilization of renewable energy systems. According to the most recent REN21 report, renewable energy accounted for 29.90% of the world's electricity usage, while the share of solar heat amounted to only as much as 1.20% [1]. Although solar energy is expanding rapidly compared to other renewable sources, it still makes up a small fraction (approximately 2%) of the total energy usage [2]. In photovoltaic (PV) technology, the solar energy absorbed by a PV module undergoes conversion into heat (in fact, internal energy), causing a rise in the PV cell's temperature, negatively impacting the PV performance and lifetime of the modules. Research shows that a PV cell efficiency decreases about 0.45% for an increase of 1 °C in cell temperature for crystalline silicon (c-Si) based solar cells [3]. It is important to note that this reduction may vary within the range of 0.30–0.45%, depending on the specific cell technology employed. Conversely, it has been observed that cooling can have a positive impact on cell efficiency [4]. To address this challenge, it is possible to enhance the performance of PV cells by integrating a cooling mechanism and utilizing an appropriate fluid (either air or liquid). This cooling process effectively lowers the PV cell temperature, avoiding the decrease in efficiency, while generating valuable thermal energy as a byproduct from the same collector area. These photovoltaic-thermal (PVT) collectors are gaining attention due to their dual capability of generating both heat and electricity simultaneously from a single renewable energy source as depicted in Fig. 1, where the PV module generates electricity directly from sunlight using semiconductor materials, while the solar thermal (ST) module extracts the waste heat from the top to heat the working fluid which flows mostly below the PV module. The warm fluid output can then be used for various heating applications such as domestic hot water (DHW), space heating (SH), drying, cooling, desalination, etc [5]. Globally, researchers and scholars are dedicating significant attention to this technology due to its numerous benefits compared to standalone PV or ST systems [6], mainly on liquid PVT systems since the early 2000s [7]. The integration of two different modules not only optimizes space utilization but is also a cost-effective solution to meet energy demands, without affecting the environment [8]. Yet, PVT systems, despite their aim to capture both electrical and thermal energy from sunlight, are more complex than standalone PV or solar thermal systems. Despite the efficiency of the thermal component in PVT systems is often lower than that of dedicated solar thermal systems, the total efficiency, encompassing both electrical and thermal components, surpasses that of solar thermal systems.

* Corresponding author.
E-mail address: z.ulabdin@tudelft.nl (Z. Ul-Abdin).

https://doi.org/10.1016/j.solener.2024.112687
Received 27 February 2024; Received in revised form 15 May 2024; Accepted 7 June 2024
Available online 15 June 2024

Nomenclature

Abbreviations

APE	avoided primary energy
DHW	domestic hot water
$KGPV$	Köppen-Geiger-Photovoltaic
LQR	linear-quadratic regulator
NTU	number of transfer units
PID	proportional–integral–derivative
PV	photovoltaic
PVT	PV-thermal
SH	space heating
ST	solar thermal

Symbols

A_{mod}	module area (m^2)
$\mathscr{B}$	packing factor
C	specific heat capacity (J kg^{-1} K^{-1})
d_{hyd}	hydraulic diameter (m)
E	input power required to operate the heat pump (W)
G	solar irradiance (Wm^{-2})
h	heat transfer coefficient (W m^{-2} K^{-1})
$\mathscr{H}_{\mathscr{A}}$	additional or auxiliary heat power (W)
$\mathscr{H}_{\mathscr{L}}$	heat losses through tank walls (W)
$\mathscr{H}_{l}$	heat removal to cover DHW demand (W)
$\mathscr{H}_{m-ta}$	heat addition from collector to storage tank (W)
ℓ	thickness of a component (m)
L	length of the module (m)
L_c	characteristic length (m)
$\mathscr{L}_{ta}$	overall heat loss coefficient of the storage tank (W m^{-2} K^{-1})
$\dot{m}$	mass flow rate (kg s^{-1})
M	mass (kg)
$\mathscr{P}$	power (W)
$\mathscr{P}_s$	available solar power (W)
Q_h	useful heat transfer for heating (W)
T	temperature (K)
V_w	wind speed (m s^{-1})
w	width of air channel (m)
W	width of the module (m)

Greek letters

α	absorptance
β	thermal expansion coefficient, 1/T (K^{-1})
β_p	temperature coefficient of maximum power, K^{-1}
δ	solar radiation coefficient
ϵ	heat exchanger effectiveness
ε	emissivity
η	efficiency
λ	thermal conductivity (W m^{-1} K^{-1})
μ	dynamic viscosity (N s m^{-2})
ρ	density (kg m^{-3})
σ	Stefan–Boltzmann constant (= 5.67×10^{-8} W m^{-2} K^{-4})
τ	transmissivity

Subscripts

am	ambient
c	conductive
cf	confined air space
el	electrical
$\mathscr{F}$	air fluid in upper channel
f	air fluid
g	glass cover
$\mathscr{G}$	top glass cover
$\mathscr{C}$	bottom glass cover
i	insulator
l	load
lp	lower absorber
p	metal plate
pv	PV cell
r	radiative
red	reduced
t	tedlar
ta	tank
th	thermal
up	upper absorber
v	convective
w	water fluid

Mostly, air or water is used as a working fluid with different arrangements of air channels, tubes, flow designs, circulation, etc. Flat-plate collectors stand out as one of the most popular and straightforward designs [9]. The use of water as a working fluid is considered more efficient compared to air because of high thermal conductivity and heat capacity [10]. This water is usually mixed with glycol in order to prevent corrosion and avoid freezing, particularly in case of colder temperatures. On the other hand, an advantage of air-based systems is their protection from fluid freezing or leaking, although a drawback is their reduced efficiency when operating in colder climates [11]. Air-based systems are particularly well-suited for drying, SH and electricity production whereas water-based systems are commonly used for water heating, cooling and industrial processes. Furthermore, the unglazed type configuration is good at producing electricity, but its ability to effectively generate heat is not so good when it comes to heating things up [12]. The performance of a PVT collector has been investigated both numerically and experimentally. Hegazy [13] did an extensive investigation of the thermal and electrical performances of flat plate air-based PVT collectors considering different configurations. However, heat transfer is quasi-steady and one-dimensional (1d) for the presented numerical models and only daily performance was evaluated. A comparative study of different configurations of air-based PVT collectors has been done under the meteorological conditions of Algiers, Algeria by Slimani et al. [14]. The numerical model incorporates the heat balance equations while considering a range of thermal and electrical parameters and the results indicate that the daily average of overall energy efficiency reaches between 30% and 74%, for a sunny day in summer depending on the inlet temperature. A comparative analysis has been carried out by Agrawal and Tiwari [15] of PVT air collectors for the composite climate of Srinagar in India. A steady-state approach has been used and only the mathematical expressions for fluid are

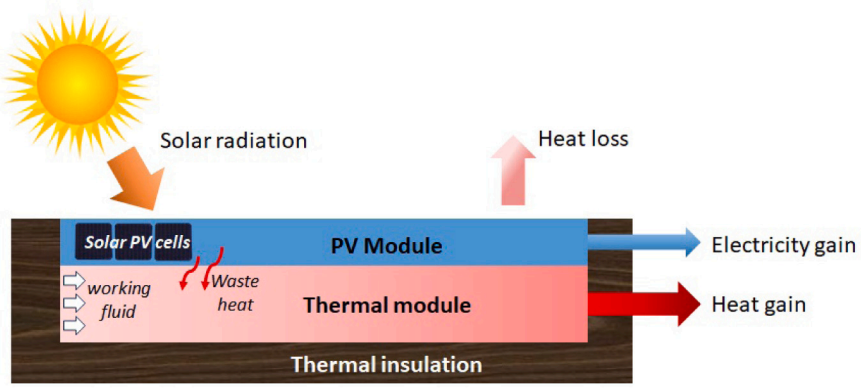

Fig. 1. Schematic diagram of a PVT collector featuring integrated PV and thermal modules for simultaneous electricity generation and heat capture.

presented for the thermal models. The performance of an air-based PVT system is influenced by important parameters such as solar irradiation intensity, inlet temperature, flow rate, and channel depth.

In a bi-fluid collector, water and air flow simultaneously and combine the advantages of air and water-based collectors with a total efficiency of up to 70%, respectively Ma et al. [16]. However, these collectors are slightly more expensive and complex than typical air-based or water-based collectors. An experimental study was conducted by Ji et al. [17] where the collector works in different working modes according to the seasonal requirements. The daily thermal efficiency found was 44% with 10.50% PV efficiency in air heating mode while 57% thermal and 11.50% PV efficiencies were achieved in water heating mode. In another experimental study carried out by Ma et al. [16], a steady-state mathematical model is also developed for a bi-fluid solar collector to analyze the daily performance. It was found that depending on the inlet temperature, the daily thermal efficiency reached was between 50% to 55%, respectively.

The collected heat could be dissipated into the environment if it is not stored, resulting in lower system efficiency and energy waste. A combination with a hot water storage tank is a compelling solution for residential buildings, where electricity and low-temperature heat are both needed. Consistent year-long demand for DHW remains constant for a single-family [18]. Combining storage tank for excess heat storage can lead to benefits such as increased system efficiency, reduced energy waste, and improved economic viability [19]. The cost of hot water storage will depend on the type, size and quality of the materials used. Installing the storage tank underground is another option but has several drawbacks such as higher cost, difficult to access for maintenance and repair. Additionally, during the winter season, the temperature drops significantly and to counteract this, space heating is required to raise the indoor temperature. This can be covered via a storage tank option or through a PVT module combined with heat pumps as a backup which consume very little electricity and are more sustainable solution financially [20]. Based on a simple 1d model representing the dynamics of the air-based collector, a Proportional–Integral–Derivative (PID) type controller is proposed by Ul Abdin and Rachid [21] and proven to guarantee good performance. However, the model was identified for a few operating points with two different values of air flow rate. Numerous control approaches based on neural networks have also been implemented in order to control the output temperature of the collector [22,23]. In colder climates (e.g. Northern Europe) much of the domestic energy demand is for heating in winter. The current shift from natural gas to electric heat pump contributes to net-congestion. Solar thermal (and PVT) in combination with seasonal heat storage, could alleviate that problem.

Most of the studies found in the literature predicting the component temperatures of the PVT modules are based on quasi-steady approaches, where the collector is considered to operate under steady-state conditions. A few studies have incorporated the dynamic response of the collector to some extent but are predominantly centered around daily simulations. However, in this study, dynamic thermal models are presented in order to estimate temperature distribution and obtain a realistic and reasonable annual performance of the system. Real weather data for different cities based on Köppen-Geiger-Photovoltaic (KGPV) climate zones is used to accurately predict the annual PV and thermal performance of the system. Simulations were carried out to validate and demonstrate the accuracy and viability of these models by comparing the results found in the literature. Extensive existing research on water-based PVT collectors with different flow passages and configurations suggests a well-explored area [24–27], making the comparison of bi-fluid collector with air-based collectors potential contributions to a less-explored domain. This paper not only provides electrical and thermal energy production by the PVT collectors but also presents a novel bi-fluid PVT system for supplying DHW, SH and PV power to a representative residential household. A control system is utilized to manage the temperature of the air outlet for space heating. H-infinity control technique has been applied to the bi-fluid PVT system which is an advanced control approach and is focused on controlling the air outlet temperature by varying the air mass flow rate. The external variations (disturbances), including solar irradiance (G), wind speed (V_w), and ambient temperature (T_{am}) are particularly challenging to manage effectively, as the classical Linear Quadratic Regulator (LQR) control scheme may fall short in comparison to the robustness offered by the H-infinity control approach. The developed dynamic models are further incorporated into the Photovoltaic Materials and Devices (PVMD) toolbox [28], which can already predict the energy yield of PV systems, expanding its functionality.

The remainder of the paper is structured as follows. The numerical models of four different PVT configurations are described in Section 2. This section also discusses the heat transfer coefficients and efficiency of the collectors. In Section 3, a new design of a bi-fluid based PVT system in combination with water storage tank and a controller for a small residential house is discussed. Finally, the main results from the present study are reported, together with a relevant discussion and validation, in Section 4, and the paper ends with conclusions and some perspectives.

2. Modeling of the PVT collectors

In this section, different configurations of air-based collectors along with a bi-fluid PVT collector are presented and illustrated in Fig. 2. The standard PV module comprises components such as a protective glass cover with PV cells immersed in a polymer layer ethylene vinyl acetate (EVA), and tedlar. These panels are extremely cheap. The first configuration, an air-based unglazed PVT presented in Fig. 2(a), is composed of standard PV module, an air channel through which the heat extraction medium air flows, and finally, an insulator to reduce

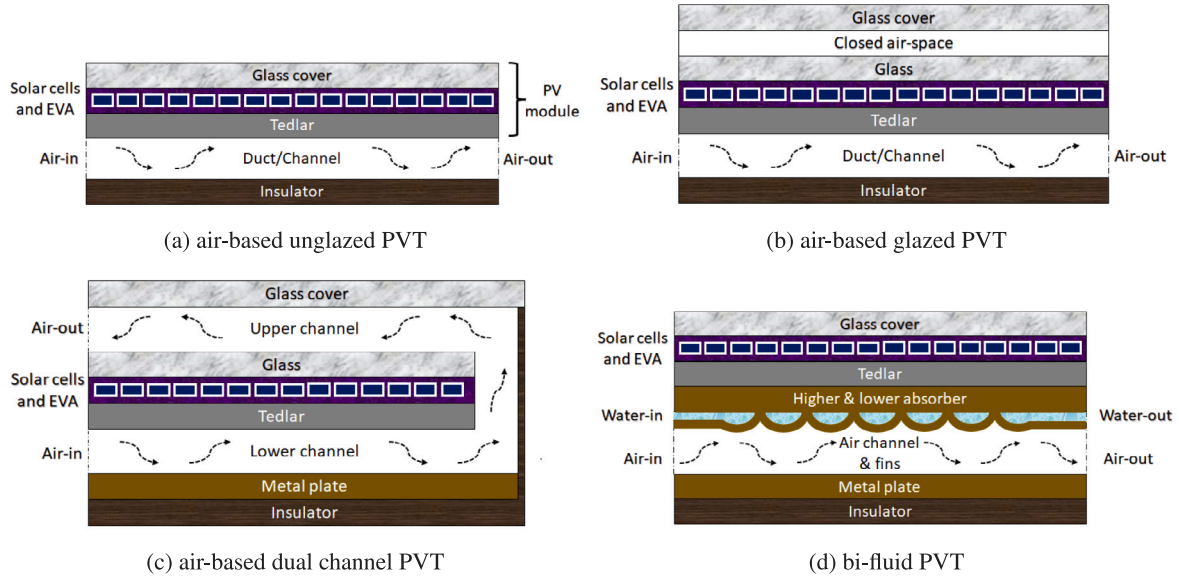

Fig. 2. Schematic cross-sectional view of the PVT collectors.

thermal losses while simultaneously improving structural strength. In the second configuration depicted in Fig. 2(b), additional glass cover with an air gap is incorporated into air-based unglazed PVT systems to minimize heat losses resulting from convection and radiation. This helps to retain the heat collected from the thermal component of the module and the system can provide more usable energy for heating purposes, such as SH or DHW. In the third configuration shown in Fig. 2(c), an additional air channel is incorporated at the top of the unglazed PVT module where outlet of the lower channel is the inlet of the upper channel. In this way, the fluid circulates within the module for a longer time and captures most of the heat which results in higher overall efficiency compared to single-channel collectors. The inlet and outlet ends of the collector are at the same end in this configuration. The last configuration of the collector (Fig. 2(d)) consists of PV module, water tubes and an air channel with an absorber plate. Here, two separate fluids circulate simultaneously and the usage of two fluids not only enhances the thermal efficiency but also enhances the electrical efficiency of the PV module by reducing the temperature of the PV cells. Moreover, for the presented configurations, metallic fins with high thermal conductivity can be added to increase the heat transfer surface area [29].

The models exhibit high nonlinearity, introducing significant challenges in the formulation of the PVT models. The following aspects have been neglected for the thermal models: pressure losses in the fluid channels, edge losses, partial shading, and dust. Radiative heat transfer between the ground and the modules is also over-sighted due to the temperature difference at the bottom being small. Additionally, the temperature of each component of the solar collector is assumed to be homogeneous and temperature distribution of every component in the horizontal direction is neglected. Finally, at the surface, the boundary conditions remain uniform for solar irradiance, wind speed, and ambient temperature. The mentioned assumptions are indeed part of the model's simplifications, it is essential to emphasize that these assumptions are considered minor in the context of the overall model.

In order to predict the temperatures and evaluate both the electrical and thermal performances of the collectors, the fundamental principle of energy conservation is applied to each component considering conductive, convective and radiative thermal exchanges between the components, which can be represented by the following equation.

$$M_\phi C_\phi \frac{dT_\phi}{dt} = \sum_{rec} \mathscr{E}_\phi - \sum_{los} \mathscr{E}_\phi, \tag{1}$$

where the left side represents the change in internal energy in the component ϕ, and the right side is the difference between energies received and lost by the component ϕ, through radiative, convective and conductive heat exchanges. M [kg] is the mass, C [J kg^{-1} K^{-1}] is the specific heat capacity, T [K] the temperature and dt [s] is the chosen time step. The solar radiation power absorbed by the glass cover in watt is $A_{mod}\alpha_g G$, where A_{mod} represents module area ($L * W$), α_g is the absorptance and G is the incident solar irradiance. Similarly, the energy absorbed by the PV cell layer is $A_{mod}\tau_g\alpha_{pv}G\mathscr{B}$. Here, τ_g represents the transmittance of the glass cover, α_{pv} is the absorptance of the PV cell, and $\mathscr{B}$ is packing factor.

2.1. Unglazed PVT collector

The governing dynamic energy balance equations for each component of the unglazed air-based PVT collector depicted in Fig. 2(a) can respectively be written as:

for glass cover (g):

$$M_g C_g \frac{dT_g}{dt} = A_{mod}[\alpha_g G + h_r^{g-s}(T_s - T_g) + h_v^{am}(T_{am} - T_g) - h_c^{g-pv}(T_g - T_{pv})], \tag{2}$$

where the sky temperature T_s for a clear sky and overcast day is given by Algarni and Nutter [30]:

$$T_s = \begin{cases} 0.0552T_{am}^{1.5}, & \text{for clear sky} \\ T_{am}, & \text{for overcast day} \end{cases} \tag{3}$$

for PV cell layer (pv):

$$M_{pv} C_{pv} \frac{dT_{pv}}{dt} = A_{mod}[\tau_g\alpha_{pv}G\mathscr{B} + h_c^{pv-g}(T_g - T_{pv}) - h_c^{pv-t}(T_{pv} - T_t)] - \mathscr{P}_{el} \tag{4}$$

Let us recall that the electric power $\mathscr{P}_{el}$ generated by the PV component of the PVT system can be expressed as follows:

$$\mathscr{P}_{el} = \mathscr{P}_s \eta_{el}, \tag{5}$$

where the available solar energy on the tilted surface, is calculated by,

$$\mathscr{P}_s = G A_{mod} \tag{6}$$

for tedlar layer (t):

$$M_t C_t \frac{dT_t}{dt} = A_{mod}[\tau_g\alpha_t G(1-\mathscr{B}) + h_c^{t-pv}(T_{pv} - T_t) + h_v^{t-f}\mathscr{X}(T_f - T_t) - h_r^{t-i}\mathscr{X}(T_t - T_i)], \tag{7}$$

where the ratio of air duct area to module area is expressed by $\mathscr{Z}$;

$$\mathscr{Z} = \frac{A_{duc}}{A_{mod}}$$

for air flowing in air channel (f):

$$\dot{m}_f C_f \frac{dT_f}{dx} = w[-h_v^{f-t}(T_f - T_t) - h_v^{f-i}(T_f - T_i)], \tag{8}$$

Using $L = 0$, $T_f = T_{f,in}$ and solution of (8) can be written as Ul Abdin and Rachid [21]:

$$T_f(L) = [(T_{f,in} - \mathscr{W})e^{-\psi} + \mathscr{W}], \tag{9}$$

where

$$\mathscr{W} = \frac{T_i h_{v,ft} + T_i h_{v,fi}}{h_{v,ft} + h_{v,fi}} \tag{10}$$

and

$$\psi = w\left(\frac{h_v^{f-t} + h_v^{f-i}}{\dot{m}_f C_f}\right) L \tag{11}$$

for insulator (i):

$$M_i C_i \frac{dT_i}{dt} = A_{duc}[h_r^{i-t}(T_t - T_i) + h_v^{i-f}(T_f - T_i) - h_v^{am}(T_i - T_{am})], \tag{12}$$

where A_{duc} is the air channel area and this completes the thermal model of the unglazed PVT collector. A similar approach for deriving the governing equations using the aforementioned principle for various components of the PVT collector is also documented in the literature [14].

2.2. Glazed PVT collector

In a glazed PVT collector presented in Fig. 2(b), a glass cover is added on top of the PV module along with an air gap between the PV laminate and the glass cover. Since the thermal module of the glazed module is similar to the unglazed type, the Eqs. (4) to (12) remain the same for the glazed collector while the governing dynamic energy balance equations for glass components and closed air space can be expressed as:

for top glass cover ($\mathscr{G}$):

$$M_g C_g \frac{dT_{\mathscr{G}}}{dt} = A_{mod}[\alpha_g G + h_r^{\mathscr{G}-s}(T_s - T_{\mathscr{G}}) + h_v^{am}(T_{am} - T_{\mathscr{G}}) - h_v^{\mathscr{G}-cf}(T_{\mathscr{G}} - T_{cf}) + h_r^{\mathscr{G}-\mathscr{C}}(T_{\mathscr{C}} - T_{\mathscr{G}})], \tag{13}$$

for closed air space (cf):

$$M_{cf} C_{cf} \frac{dT_{cf}}{dt} = A_{mod}[h_v^{cf-\mathscr{C}}(T_{\mathscr{C}} - T_{cf}) - h_v^{cf-\mathscr{G}}(T_{cf} - T_{\mathscr{G}})], \tag{14}$$

for bottom glass cover ($\mathscr{C}$):

$$M_g C_g \frac{dT_{\mathscr{C}}}{dt} = A_{mod}[\alpha_g^2 G + h_r^{\mathscr{C}-\mathscr{G}}(T_{\mathscr{G}} - T_{\mathscr{C}}) + h_v^{\mathscr{C}-cf}(T_{cf} - T_{\mathscr{C}}) - h_c^{\mathscr{C}-pv}(T_{\mathscr{C}} - T_{pv})], \tag{15}$$

Remark: With the addition of an extra glass cover, the solar radiation energy absorbed by the bottom glass is $A_{mod}\alpha_g^2 G$ whereas the energy absorbed by the PV cell layer is $A_{mod}\tau_g^2\alpha_{pv}G\mathscr{B}$.

Remark: In a glazed PVT collector, the conductive heat exchange takes place between the bottom glass and the cell layer.

2.3. Dual channel PVT collector

In a dual channel PVT collector, an air duct is added on top of the PV module whose inlet temperature is the outlet of the lower channel as illustrated in Fig. 2(c). The governing dynamic energy balance equations for the upper air channel and metal plate of the collector can be expressed as:

for air flowing in upper channel ($\mathscr{F}$):

$$\dot{m}_f C_f \frac{dT_{\mathscr{F}}}{dx} = w[-h_v^{\mathscr{F}-\mathscr{G}}(T_{\mathscr{F}} - T_{\mathscr{G}}) - h_v^{\mathscr{F}-\mathscr{C}}(T_{\mathscr{F}} - T_{\mathscr{C}})], \tag{16}$$

where the solution of (16) can be written as:

$$T_{\mathscr{F}}(L) = [(T_f(L) - \varpi)e^{-\vartheta} + \varpi], \tag{17}$$

where

$$\varpi = \frac{T_{\mathscr{G}} h_v^{\mathscr{F}-\mathscr{G}} + T_{\mathscr{C}} h_v^{\mathscr{F}-\mathscr{C}}}{h_v^{\mathscr{F}-\mathscr{G}} + h_v^{\mathscr{F}-\mathscr{C}}} \tag{18}$$

and

$$\vartheta = w\left(\frac{h_v^{\mathscr{F}-\mathscr{G}} + h_v^{\mathscr{F}-\mathscr{C}}}{\dot{m}_f C_f}\right) L, \tag{19}$$

where $T_f(L)$, is the outlet air temperature of the lower channel and is given in (9).

for metal plate (p):

$$M_p C_p \frac{dT_p}{dt} = A_{duc}[h_c^{p-i}(T_i - T_p) + h_v^{p-f}(T_f - T_p) - h_r^{p-t}(T_p - T_t)], \tag{20}$$

Remark: In dual channel PVT collector, the convective heat exchange between the two glasses and fluid flowing in the upper channel ($\mathscr{F}$) is different from the fluid in closed air space (cf) and the two glasses.

Remark: T_f in dual channel is the temperature of lower channel fluid and the output air of lower channel $T_f(L)$ is the inlet of the above channel.

Remark: It should be noted that in this model, the convective heat exchange takes place between the fluid and the metal plate and not between the fluid and insulator as mentioned in the previous models.

Remark: Here, radiative heat exchange occurs between the tedlar and metal plate while conductive heat exchange takes place between the metal plate and the insulator.

2.4. Bi-fluid PVT collector

In a bi-fluid PVT collector as depicted in Fig. 2(d), a water channel is added to the thermal module. Since the electrical module here is similar to the unglazed air-based collector, the Eqs. (2) to (7) remain the same and the governing dynamic energy balance equations for absorbers and fluid channel are given as:

for upper absorber (up):

$$M_{up} C_{up} \frac{dT_{up}}{dt} = A_{mod}[h_c^{up-t}(T_t - T_{up}) + (1-\xi)h_c^{up-lp}(T_{lp} - T_{up}) + \xi h_r^{up-lp}(T_{lp} - T_{up})] + A_w h_v^{up-w}(T_w - T_{up}), \tag{21}$$

where, ξ is the percentage of collector occupied by channel.

for water channel (w):

$$M_w C_w \frac{dT_w}{dt} = A_w[h_v^{w-up}(T_{up} - T_w) + h_v^{w-lp}(T_{lp} - T_w)] + \dot{m}_w C_w(T_w - T_{w,in}), \tag{22}$$

It is assumed that the water temperature (T_w) in the water channel is the mean of the water inlet temperature ($T_{w,in}$) and water outlet temperature ($T_{w,o}$), the outlet temperature is calculated by Ul Abdin [31]:

$$T_{w,o} = 2T_w - T_{w,in} \tag{23}$$

for lower absorber (lp):

$$M_{lp} C_{lp} \frac{dT_{lp}}{dt} = A_{mod}[(1-\xi)h_c^{lp-up}(T_{up} - T_{lp}) + \xi h_r^{lp-up}(T_{up} - T_{lp}) + h_r^{lp-p}(T_p - T_{lp}) + h_v^{lp-f}(T_f - T_{lp})] + A_w h_v^{lp-w}(T_w - T_{lp}), \tag{24}$$

Remark: In this model, conductive heat exchange occurs between the tedlar and upper absorber instead of convective heat exchange between the tedlar and the fluid.

Remark: Finally, convective heat exchange takes place between the lower absorber and the air fluid flowing below and radiative heat exchange between the lower absorber and metal plate above the insulator.

2.5. Heat transfer coefficients

The convective heat coefficient strongly depends on the wind speed V_w and is defined by the following equations [32].

$$h_v^{am} = \begin{cases} 5.7 + 3.8V_w, & \text{for } V_w < 5 \text{ ms}^{-1} \\ 6.47 + {V_w}^{0.78}, & \text{for } V_w > 5 \text{ ms}^{-1} \end{cases} \tag{25}$$

The radiation heat transfer coefficient between the atmosphere and the top glass cover of the module is Alsaqoor et al. [33];

$$h_r^{g-s} = \sigma\varepsilon_g(T_g + T_s)(T_g^2 + T_s^2), \tag{26}$$

where σ is the Stefan Boltzmann constant. Radiative heat transfer between two parallel elements a and b is Singh et al. [34];

$$h_r^{a-b} = \sigma\left[\frac{(T_a + T_b)(T_a^2 + T_b^2)}{\frac{1}{\varepsilon_a} + \frac{1}{\varepsilon_b} - 1}\right], \tag{27}$$

where ε_a and ε_b are the emissivities of the two components. Conductive heat transfer coefficient between two parallel layers a and b is given as Slimani et al. [14];

$$h_c^{a-b} = \frac{1}{\frac{\ell_a}{\lambda_a} + \frac{\ell_b}{\lambda_b}} \tag{28}$$

Convective heat transfer coefficient between two elements is Vajedi et al. [35];

$$h_v^f = N_u\frac{\lambda_f}{d_{hyd}}, \tag{29}$$

where N_u is the Nusselt number and one can calculate it as follows;

$$N_u = 0.023R_e^{0.8}P_r^{0.4} \tag{30}$$

here R_e and P_r are the Reynolds number R_e and Prandtl number P_r, respectively:

$$R_e = \frac{\rho_f d_{hy}}{\mu_f}V_f \tag{31}$$

and

$$P_r = \frac{\mu_f}{\lambda_f}C_f \tag{32}$$

The convective heat transfer coefficient in an enclosed air space [36] is:

$$h_v^{cf} = \frac{N_u^{cf}\lambda_{cf}}{\ell_{cf}}, \tag{33}$$

where N_u^{cf} is the Nusselt number characterizing the natural convection of the air confined between glass and PV module and is determined using K. Hollands's correlation [37]:

$$N_u^{cf} = \left[1 + 1.44\left(1 - \frac{1708}{R_a\cos\theta}\right)^*\left(1 - \frac{1708(\sin 1.8\theta)^{1.6}}{R_a\cos\theta}\right) + \left(\left(\frac{R_a\cos\theta}{5830}\right)^{1/3} - 1\right)^*\right] \tag{34}$$

with Rayleigh number, given by

$$R_a = \frac{g\beta\Delta T L_c^3\rho_{cf}^2 C_{cf}}{\lambda_{cf}\mu_{cf}} \tag{35}$$

The brackets signified by the superscript * go to zero when they are negative.

2.6. Efficiencies

This section discusses the performance of the PVT collectors in terms of thermal, electrical, total efficiency and avoided primary energy (APE) consumption. The thermal and electrical performance of air-based PVT collector is Slimani et al. [14], Yu et al. [38];

$$\eta_{el} = \eta_{el,ref}\left[1 + \beta_p(T_{pv} - T_{pv,ref}) + \delta ln\frac{G}{G_{ref}}\right], \tag{36}$$

where the PV module utilizes Mono Crystalline Silicon PV cells, with a reference electrical efficiency of 15% at the standard testing conditions (G_{ref}: 1000 Wm^{-2}, $T_{pv,ref}$: 25 °C and V_w: 0 ms^{-1}). The temperature coefficient (β_p) is −0.45%/K and solar radiation coefficient (δ) is 0.052. The selection of 15% for PV module electrical efficiency might appear conservative; nevertheless, it is essential to note that in this scenario, PV modules are integrated with thermal modules, forming a PVT collector. This integration impacts overall efficiency due to additional losses introduced by the thermal component, beyond pure electrical output. Additionally, the 15% figure provides a more practical estimate for PVT applications compared to standalone PV modules.

$$\eta_{th} = \frac{\dot{m}C(T_o - T_i)}{\mathscr{P}_s}, \tag{37}$$

where T_i and T_o are the inlet and outlet temperatures of the circulating fluid.

In the case of the bi-fluid, the total thermal efficiency of the collector is calculated as follows:

$$\eta_{th,tot} = \frac{\dot{m}_f C_f(T_{f,o} - T_{f,in}) + \dot{m}_w C_w(T_{w,o} - T_{w,in})}{\mathscr{P}_s} \tag{38}$$

Slimani et al. [14] proposed an expression to compute the overall thermal efficiency of a PVT collector, considering the distinct nature of thermal and electrical energy. The C_{pf} denotes the electrical generation efficiency of a conventional power plant, which typically ranges from 0.20 to 0.40, dependent on the quality of coal used [39].

$$\eta_{ov} = \eta_{th} + \frac{\eta_{el}}{C_{pf}} \tag{39}$$

It is important to keep in consideration that a PVT collector has the unique capability of generating both heat and electricity simultaneously. Hence, the cumulative energy output of a PVT system per square meter surpasses the individual yields of the reference systems per square meter [12]. To put it in simpler terms, 1 kWh of electrical energy is not equivalent to 1 kWh of thermal energy and their combination should not be simply summed up. The energy performance is measured by the amount of primary energy saved, referred to as avoided primary energy consumption, defined as:

$$APE = \frac{\mathscr{P}_{th}}{\eta_{pr,th}} + \frac{\mathscr{P}_{el}}{\eta_{pr,el}}, \tag{40}$$

where $\mathscr{P}_{th}$ and $\mathscr{P}_{el}$ are the thermal and electrical energy of the PVT collectors and the numerical values used for the parameters are:

- $\eta_{pr,th}$ is a measure of how well a conventional gas-fired DHW system can turn heat into useful energy and it is usually around 65% [12].
- $\eta_{pr,el}$ is the power generation efficiency of a conventional power plant, assumed equal to 40% [40].

The total reduction in conventional gas usage resulting from the implementation of the PVT collector is computed by considering the localized decrease in demand for natural gas primarily used for DHW and SH purposes.

3. Innovative design of bi-fluid PVT system

There are multiple ways to design the integration of a storage tank with a PVT collector, depending on the application and system requirements. By storing excess thermal energy produced by the collector, it is possible to reduce the dependence on auxiliary heaters, which might otherwise be required during periods of low solar irradiation. The aim of this work is simultaneous use of domestic applications such as DHW, SH and to give a realistic model in order to obtain reasonable performance of the system.

3.1. System description

In this section, a novel bi-fluid PVT system has been employed for DHW and SH. A bi-fluid type PVT collector, as described in the previous section, is combined with a storage tank and a robust controller. The collector functions by allowing air and water to circulate simultaneously beneath the PV module. The heat extracted from the top of the collector is transferred to the storage tank fluid for DHW purposes. A closed-loop serpentine tube is utilized, which is connected to a heat exchanger. This heat exchanger efficiently transfers the collected heat to the storage tank fluid to be used for DHW. Meanwhile, when the heating is required, the warm air at the outlet end of the collector is channeled into a controller. This controller ensures that the air attains the desired temperature of 21 °C, facilitating its usage for SH. Fig. 3 presents the schematic view of the system that is composed of several components:

- a PV module which consists of a glass cover, PV cells and a protective tedlar layer. This module generates electricity to current system (power pumps, auxiliary heaters) and electrical load
- a thermal module which consists of a water and an air channel in order to produce both warm air and hot water
- a storage tank where warm fluid coming from the collector is stored for later use
- a heat exchanger, to transfer the heat collected by the closed-loop serpentine tube from the collector to the fluid inside the storage tank
- circulation pumps, to circulate the fluids within the system, ensuring a continuous flow through the collector
- an H-infinity based robust controller to provide the desired air temperature when needed
- back up electric auxiliary heaters, to provide additional heating support when the solar energy collected by the collector is insufficient.

A pump can be eliminated by relying on natural convection for fluid circulation, reducing electricity consumption, operational costs and simplifying the system. The electrical energy generated by the PV module can be added to the grid when there is excess and energy can be drawn from the grid at a later time.

A few assumptions have been taken into account for the proposed system, such as:

- PVT collector is assumed to be well-insulated, with no significant heat losses to the surroundings
- constant fluid properties, within the operating temperature range
- losses at bends, valves, and other components in the absorber plates are over-sighted
- the flow rate of the fluid within the module remained constant across all pipes
- uniform temperature and composition throughout the tank
- pressure drops and losses across the components of the system are assumed to be negligible.

3.2. Integration of water storage tank

The provision of hot water demand is met through a combination of the auxiliary heater and PVT system. To ensure a continuous supply, an adeptly designed water tank serves as a crucial energy storage component for storing the heated water. The tank is assumed as a fully mixed, the temperature is evenly distributed, eliminating any variations and the energy balance on the tank is discretized in time, such that the water temperature in the tank at each time step $T_{ta}(i+1)$ is determined based on multiple heat fluxes from the preceding time step, that is,

Storage tank (ta):

$$T_{ta}(i+1) = T_{ta}(i) + \frac{\dot{\mathscr{H}}_{m-ta}(i) - \dot{\mathscr{H}}_{l}(i) - \dot{\mathscr{H}}_{\mathscr{L}}(i)}{M_{ta}C_{w}}\Delta t, \tag{41}$$

where Δt is the time step and $\dot{\mathscr{H}}_{m-ta}$ is the energy transferred from the PVT collector to the tank through the heat exchanger of effectiveness ϵ and can be expressed as

$$\dot{\mathscr{H}}_{m-ta}(i) = \epsilon \dot{m}_{w} C_{w}(T_{m,\mathscr{O}}(i) - T_{ta}(i)), \tag{42}$$

The temperature at the exit of the heat exchanger submerged in the tank, $T_{\mathscr{X}}$, is,

$$T_{\mathscr{X}}(i) = T_{m,\mathscr{O}}(i) - \epsilon[T_{m,\mathscr{O}}(i) - T_{ta}(i)], \tag{43}$$

The heat exchanger's effectiveness can be predicted directly from the heat exchanger characteristics and relevant flows, assuming constant temperature on one side. The calculation is then derived from Herrando et al. [41]:

$$\epsilon = 1 - exp^{-NTU}, \tag{44}$$

where NTU, is a dimensionless parameter and it relates the heat capacity rates and heat transfer surface area to evaluate the degree of heat exchange between the two fluids.

Since the system operates as a closed loop, this temperature will also serve as the inlet temperature for the collector in the subsequent time step,

$$T_{m,in}(i+1) = T_{\mathscr{X}}(i) \tag{45}$$

Similarly, $\dot{\mathscr{H}}_{l}$ is the energy required to meet the demand for DHW and can be represented as

$$\dot{\mathscr{H}}_{l}(i) = \dot{m}_{l} C_{w}(T_{ta,in}(i) - T_{ta}), \tag{46}$$

It is important to highlight that the fluid leaving the heat exchanger and entering the collector experiences no heat loss or heat gain and the mass flow rates are equal.

The heat losses through the walls $\dot{\mathscr{H}}_{\mathscr{L}}$ at time step i can be found from

$$\dot{\mathscr{H}}_{\mathscr{L}}(i) = A_{ta}\mathscr{L}_{ta}(T_{ta}(i) - T_{am}) \tag{47}$$

Remark: Heat is supplied to the storage tank solely when the temperature of the water exiting the collector $T_{m,\mathscr{O}}(i)$ surpasses that of the water in the tank $T_{ta}(i)$. In the absence of this condition, no heat is added, implying $\dot{\mathscr{H}}_{m-ta} = 0$.

Remark: $\dot{\mathscr{H}}_{l}$ equals zero when the inlet temperature of the storage tank $T_{ta,in}(i)$ exceeds the storage tank's current temperature $T_{ta}(i)$.

Remark: If the fluid temperature at the leaving point of the collector $T_{m,\mathscr{O}}(i)$ is higher than inlet temperature $T_{m,in}(i+1)$ but lower than the fluid temperature in the storage tank $T_{ta}(i)$, bypass is activated, the pump circulates the fluid through the PVT collector without adding more heat to the storage tank, such that $T_{m,in}(i+1) = T_{m,\mathscr{O}}(i)$. By doing this, the storage tank is prevented from cooling down.

3.3. Controller design

A robust H-infinity controller was adopted to control the outlet air temperature at around 21 °C when heat is required. A separate control

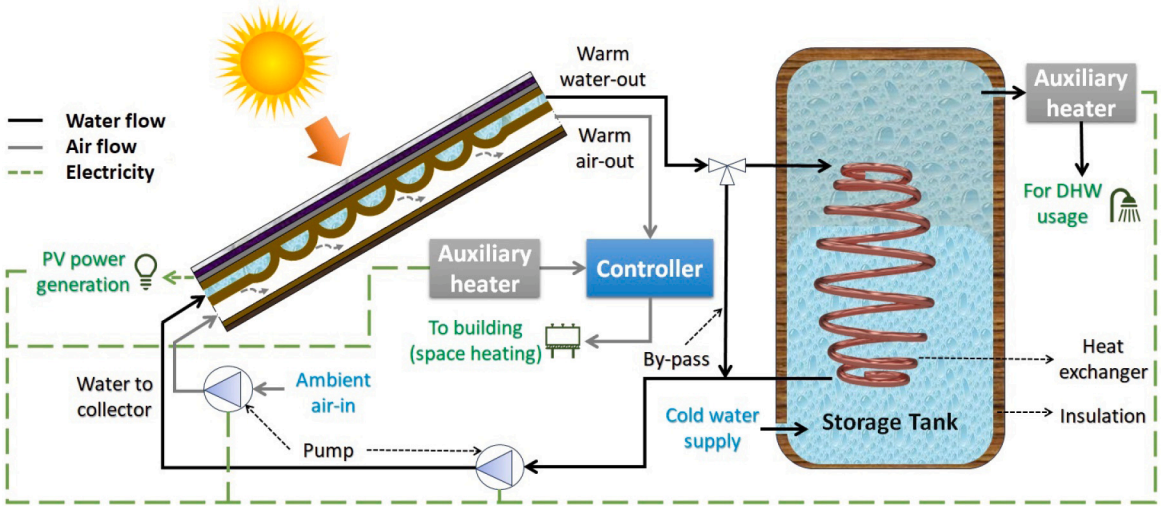

Fig. 3. Schematic diagram of a novel bi-fluid PVT system coupled with a storage tank, auxiliary heaters and a controller.

system is considered to maintain the air outlet temperature because there is no storage tank in this setup for air output. The only control variable is the air mass flow rate. H-infinity control methodology is designed to provide a higher degree of robustness in the presence of disturbances, uncertainties, and modeling errors. It minimizes the worst-case impact of disturbances on the system's performance, making it ideal for complex systems with unpredictable variations. The disturbances identified in this case are solar irradiance, wind speed and ambient temperature.

The initial nonlinear thermal model of the collector is expressed in the form

$$\dot{x} = f(x,u,d) \qquad x\epsilon\mathbb{R}^m, u\epsilon\mathbb{R}^n, d\epsilon\mathbb{R}^q \tag{48}$$

where u is the control input, specifically denoting the mass flow rate in this case, d contains the external disturbances with bounded values

$$d = \begin{bmatrix} G & T_{am} & V_w \end{bmatrix}^T \tag{49}$$

these disturbances are presumed to be well-defined. The state vector x comprises the temperatures of individual layers, serving as the state variables, and is formulated as follows:

$$x = \begin{bmatrix} x_1 & x_2 & x_3 & x_4 & x_5 & x_6 & x_7 & x_8 \end{bmatrix}^T = \begin{bmatrix} T_g & T_{pv} & T_t & T_{up} & T_w & T_{lp} & T_p & T_i \end{bmatrix}^T \tag{50}$$

The resulting output corresponds to the outlet temperature of the fluid leaving the air channel in the PVT collector.

Remark: Since the inlet temperature of the air channel in this case is assumed same as the ambient temperature, it is not considered as a separate disturbance in Eq. (49).

3.3.1. Linearization of the thermal model

At each iteration of the control process, the thermal model is linearized around its current operating point (x^*, u^*), where x^* is the present value of the system's state vector and u^* is the last sampled value of the control input that was exerted on the PVT system. The linearization procedure requires the computation of the Jacobian matrices and the dynamic model is described by

$$\dot{x} = Ax + Bu + Hd \tag{51}$$

where matrices A, B, and H are derived through the computation of the Jacobians.

$$A = \begin{bmatrix} \frac{\partial f_1}{\partial x_1} & \cdots & \frac{\partial f_1}{\partial x_8} \\ \frac{\partial f_2}{\partial x_1} & \cdots & \frac{\partial f_2}{\partial x_8} \\ \vdots & \ddots & \vdots \\ \frac{\partial f_8}{\partial x_1} & \cdots & \frac{\partial f_8}{\partial x_8} \end{bmatrix}\Bigg|_{(x^*,u^*)},$$

$$B = \begin{bmatrix} \frac{\partial f_1}{\partial u} & \frac{\partial f_2}{\partial u} & \cdots & \frac{\partial f_8}{\partial u} \end{bmatrix}^{\mathsf{T}}\Big|_{(x^*,u^*)},$$

Similarly, H is the disturbance matrix and is given by

$$H = \begin{bmatrix} \frac{\partial f_1}{\partial d_1} & \frac{\partial f_2}{\partial d_1} & \cdots & \frac{\partial f_8}{\partial d_1} \\ \frac{\partial f_1}{\partial d_2} & \frac{\partial f_2}{\partial d_2} & \cdots & \frac{\partial f_8}{\partial d_2} \\ \frac{\partial f_1}{\partial d_3} & \frac{\partial f_2}{\partial d_3} & \cdots & \frac{\partial f_8}{\partial d_3} \end{bmatrix}^{\mathsf{T}}\Bigg|_{(x^*,u^*)}$$

The above matrices define the system dynamics and the provided linearized representation of the thermal model can be effectively managed through the implementation of an advanced H-infinity control technique.

3.3.2. H-infinity feedback control

In control theory, the H-infinity controller addresses the solution of the optimal control problem in the presence of external perturbations. The solution to a min–max problem involves a scenario where perturbations aim to maximize a cost function, while control input work to minimize a cost function that includes a quadratic tracking error term for the state vector. The output is transformed into states to facilitate the controller design process. These states are identified to ensure compatibility with the desired output. Subsequently, the controller is devised with the objective of steering the system toward tracking these states. This strategic approach ultimately enables the output to accurately follow the intended target output. Fig. 4 illustrates the control scheme for the proposed bi-fluid thermal model. The reference setpoints for the state vector are defined as follows:

$$x_d = \begin{bmatrix} T_{g,d} & T_{pv,d} & T_{t,d} & T_{up,d} & T_{w,d} & T_{lp,d} & T_{p,d} & T_{i,d} \end{bmatrix}^T \tag{52}$$

By using the control input, the tracking of the setpoints is accomplished. The control input u is assumed to differ from the control input u_d at every time instant.

The disturbance effects are incorporated in the quadratic cost function. Due to the presence of a perturbation term within the system, the applicability of a classical LQR control approach becomes less

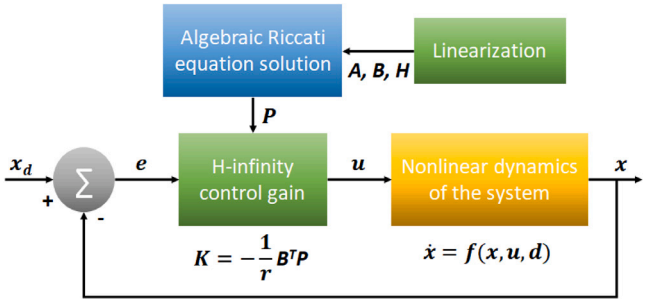

Fig. 4. H-infinity control scheme for the bi-fluid PVT thermal model.

practical in addressing this problem. Unlike the PID control method, which possesses limitations in guaranteeing control loop stability when confronted with shifts in operating points. This strategy not only addresses the challenges posed by the perturbation term but also offers robustness, ensuring stability across varying operating conditions. This control strategy, not only tracks the system's state vector but also adeptly accounts for the worst possible disturbances that have the potential to impact the collector's performance. A control signal is computed to minimize the worst possible disturbance imposed externally onto the system. Although, the optimization problem solution is directly connected to parameter ρ. Parameter ρ sets how much the disturbances affect rewards whereas parameter r systematically determines the extent to which the control input is penalized (r, $\rho > 0$). The H-infinity feedback optimal control law is expressed as Ul Abdin [31]

$$u(t) = -Kx(t), \tag{53}$$

The solution to this problem involves solving the Algebraic Riccati equation to find the optimal state feedback gain matrix K and is given by Rigatos [42]

$$K = \frac{1}{r}B^T P \tag{54}$$

where P denotes a positively semi-definite symmetric matrix, obtainable through the solution of the algebraic Riccati equation

$$A^T P + PA + Q - P\left(\frac{2}{r}BB^T - \frac{1}{\rho^2}HH^T\right)P = 0, \tag{55}$$

In this scenario, to ascertain the stabilizing feedback control, it becomes necessary to iteratively solve an algebraic Riccati equation during each step of the control algorithm. The matrix Q is characterized by its positive definite symmetric nature. Solving the Riccati equation results in the formation of a positive definite symmetric matrix P and the values of the matrix are directly influenced by the parameters ρ and r. For a solution to exist for the control problem, the parameter ρ needs to exceed the lower bound ρ_{min}. This means that the acceptable range for the value of ρ is within $[\rho_{min}, \infty]$. The structure of the controller transforms into

$$u(t) = -K(x(t) - x_d(t)) + u_d, \tag{56}$$

where x_d and u_d are the desired states and desired control input. It is essential to transform the desired output into corresponding desired states and this requires the determination of both states and control input, making $\dot{T}_g$, $\dot{T}_{pv}$, $\dot{T}_t$, $\dot{T}_{up}$, $\dot{T}_w$, $\dot{T}_{lp}$, $\dot{T}_p$, $\dot{T}_i$ and $T_{f,o} - T_{f,od} = 0$ and the solution of this system is the desired state vector x_d and control input signal u_d. Each step is described as

$$\begin{aligned} x_d &= \begin{bmatrix} x_{1,d} & x_{2,d} & x_{3,d} & x_{4,d} & x_{5,d} & x_{6,d} & x_{7,d} & x_{8,d} \end{bmatrix}^T \\ &= \begin{bmatrix} T_{g,d} & T_{pv,d} & T_{t,d} & T_{up,d} & T_{w,d} & T_{lp,d} & T_{p,d} & T_{i,d} \end{bmatrix}^T \end{aligned} \tag{57}$$

The controller is now fully structured to manage the system's response and ensure accurate tracking of the desired output.

3.4. System performance evaluation

The evaluation of a proposed novel bi-fluid PVT system's effectiveness can be assessed by considering both its generation of PV energy output and thermal energy output (for SH and supplying DHW). The fraction of electrical energy demand covered by the system is calculated using [18]

$$\mathscr{F}_{el} = \frac{\sum_{t=0}^{t=T} \mathscr{P}_{el}(t)}{\mathscr{P}_{el,dem}}, \tag{58}$$

where $\mathscr{P}_{el,dem}$ is the electrical energy required by the user. Similarly, it determines the portion of thermal energy demand covered through

$$\mathscr{F}_{th} = \frac{\sum_{t=0}^{t=T} \dot{m}_l C_w (T_{ta,in} - T_{ta})}{\sum_{t=0}^{t=T} \dot{m}_w C_w (T_{dem} - T_{ta,in})} \tag{59}$$

It should be noted that the collector's outlet fluid can flow into the storage tank as long as its temperature surpasses that of the tank temperature. Additionally, we assumed no losses in the DC to AC conversion process for PV module.

Further, an auxiliary heater is utilized to fulfill the DHW requirement whenever the temperature of the storage tank falls below the demand temperature T_{dem}, usually 60 °C. The amount of extra heat or supplementary heat required to guarantee the demand temperature level is given by

$$\dot{\mathscr{H}}_{\mathscr{A}}(i) = \dot{m}_l C_w (T_{dem} - T_{ta}(i)) \tag{60}$$

Another auxiliary heater is added to this system once the need for SH has been detected. The thermostat regulates both the auxiliary heaters and achieving precise control over them can be challenging. However, heat pumps can be added to this system to support SH when PVT is not working as they are energy-efficient and cost-effective. Air source heat pumps are better suited for areas with limited annual solar radiation [43]. They operate by transferring heat between the outdoor and indoor air, extracting heat from the outdoor air during the heating season.

The regular coefficient of performance (COP) is typically defined as the ratio of the useful heat transfer to the input energy required to operate the heat pump and is given by

$$COP_{th} = \frac{Q_h(t)}{E(t)} \tag{61}$$

where combined electricity and heating capacity coefficient of performance of a PVT collector can be obtained from Zhang et al. [44]

$$COP_{PVT} = \frac{Q_h(t) + \mathscr{P}_{el}(t)/\eta_{pr,el}}{E(t)} \tag{62}$$

The energy demand for the house during heating season can be defined as Yumrutaş and Ünsal [45]:

$$Q_h(t) = (hA)_{\mathscr{X}}(T_R(t) - T_H), \tag{63}$$

where $(hA)_{\mathscr{X}}$ is the product of the radiator surface area and heat transfer coefficient, T_R is the temperature of fluid in the radiator and T_H is desired indoor air temperature. Another possible way to express the SH load, is given by (positive values only) [46]:

$$Q_h(t) = (hA)_{\mathscr{L}}(T_H - T_{am}(t))^+, \tag{64}$$

where $(hA)_{\mathscr{L}}$ is the space loss coefficient and area product of the house. Typical value for it is in the range of 24 to 60 W/°C, considering heating floor area of 120 m^2. Let us assume a value of 42 W/°C for a well-insulated building and an outdoor ambient temperature of 0 °C, the estimated heating load to maintain an indoor temperature of 21 °C would be approximately 882 watts. We consider a heat pump with a capacity of 1 kW for some margin. COP can be influenced by various factors, including indoor, outdoor temperatures and the efficiency of the heat pump itself. The warm air can be used for SH while electrical

Table 1
The used thermo-physical properties of the studied PVT models.

	Symbol	Explanation	Value
Glass cover	α_g	Absorptivity	0.10
	C_g	Heat capacity	670 J kg^{-1} K^{-1}
	λ_g	Conductivity	1.10 W m^{-1} K^{-1}
	ρ_g	Density	2200 kg m^{-3}
	ϵ_g	Emissivity	0.88
	ℓ_g	Thickness	0.0032 m
	τ_g	Transmittance	0.84
	A_{mod}	Module area ($L \times W$)	1 × 0.50 m^2
PV cell	α_{pv}	Absorptivity	0.90
	β_p	Temperature coefficient	−0.45%/K
	C_{pv}	Heat capacity	900 J kg^{-1} K^{-1}
	δ	Solar radiation coefficient	0.052
	λ_{pv}	Conductivity	148 W m^{-1} K^{-1}
	ρ_{pv}	Density	2330 kg m^{-3}
	$\eta_{el,ref}$	Strand efficiency	15%
	ℓ_{pv}	Thickness	0.0003 m
Tedlar	α_t	Absorptivity	0.80
	C_t	Heat capacity	1200 J kg^{-1} K^{-1}
	λ_t	Conductivity	0.20 W m^{-1} K^{-1}
	ρ_t	Density	1200 kg m^{-3}
	ℓ_t	Thickness	0.00075 m
Air	C_f	Heat capacity	1007 J kg^{-1} K^{-1}
	λ_f	Conductivity	0.026 W m^{-1} K^{-1}
	ρ_f	Density	1.184 kg m^{-3}
	ℓ_{cf}	Depth of duct	0.020 m
Absorber	α_p	Absorptivity	0.95
	C_p	Heat capacity	887 J kg^{-1} K^{-1}
	λ_p	Conductivity	250 W m^{-1} K^{-1}
	ρ_p	Density	2710 kg m^{-3}
	ℓ_p	Thickness	0.001 m
Water	C_w	Heat capacity	4186 J kg^{-1} K^{-1}
	λ_w	Conductivity	0.60 W m^{-1} K^{-1}
	ρ_w	Density	998 kg m^{-3}
Insulation	C_i	Heat capacity	670 J kg^{-1} K^{-1}
	λ_i	Conductivity	0.034 W m^{-1} K^{-1}
	ρ_i	Density	20 kg m^{-3}
	ℓ_i	Thickness	0.05 m

Table 2
Validation of a bi-fluid PVT collector — water part: a comparison between this study and study done by [39].

	Analytically [39]	Proposed model [39]	This study
Mean air flow temperature [°C]	31.50	31	31
air flow outlet temperature [°C]	33	32	33

energy generated by the PV module is needed to operate the heat pump. Higher COP can be achieved if warmer air is provided by the collector. It must be taken into consideration that with a heated floor area of 120 m^2, which has approximately 2 bedrooms, one bathroom, one living-room and a kitchen, the coverage potential of the bi-fluid collector is limited. Otherwise, an additional or bigger bi-fluid collector is needed to effectively cover the entire space.

4. Results and discussion

The performance of the PVT collectors is strongly influenced by a range of parameters, such as: ambient temperature, solar irradiance, wind speed, mass flow rate, type of fluid, materials used, and the thickness of components, as outlined in Table 1. First, the models are validated by comparing the obtained results with those reported in the existing literature. This validation demonstrates that the dynamic models are accurate and reliable. Next, simulations are performed for the developed air-based models and a bi-fluid model to assess and compare the hourly performance in detail for the Amsterdam region in the Netherlands. The monthly outputs of the collectors were calculated, with the final aim of obtaining total annual yields and APE. Later, a comparison of electrical output, thermal output and APE was performed for six cities from the northern hemisphere, each representing a distinct KGPV zone. In the second part, simulations are performed for the novel bi-fluid PVT system, integrated with a storage tank for DHW and a controller for SH. The developed models have been integrated to the PVMD toolbox and the Matlab program is used for the numerical models as well as the climatic parameters.

To solve the system of ordinary differential equations (ODEs) representing the energy conservation principle for each component of a PVT collector, MATLAB's *ode23* solver is employed. The solver iteratively computes the solution by advancing the numerical approximation through small time steps. By providing initial conditions, along with the differential equations describing the energy balance for each component, *ode23* computes the temperature profiles and therefore evaluates both the electrical and thermal performances of the collectors over time. When solving ODEs numerically, smaller time steps generally lead to more accurate results. Conversely, larger time steps can significantly speed up computations but may sacrifice a bit of accuracy in predicting temperatures.

4.1. Validation and verification of PVT models

To validate and demonstrate the accuracy and viability of the above models, simulations were carried out and the obtained results (for PV cell temperature, outlet fluid temperatures and efficiencies) were compared with the results found in the literature. In order to achieve this, the PVT models presented in this study are simulated with the same operating conditions and thermo-physical properties described in literature studies. The unglazed air-based model results are compared with the experimental and numerical results found by Kim et al. [47], Das et al. [48]. Under similar ambient temperature and solar radiation profiles, it can be observed in Fig. 5(a) that the occurring differences for the air outlet temperature are less than 0.50 °C. In addition, Fig. 5(b) shows that there is good compatibility between PV cell temperatures and efficiencies obtained in the present study and reported in Das et al. [48], considering similar thermo-physical properties.

In the experimental study [49], the glazed air-based PVT modules are connected in series with an effective area of 0.61 m^2 of one PVT module and a depth of 0.02 m. The outlet of flowing air has been connected to the inlet of the second collector in the series. Similarly, the outlet of the second collector is connected to the inlet of the third collector. The validation process involves, examining the performance of a single PVT module only. The output shown in Fig. 6 shows a good resemblance between the reference experimental data and the results obtained by the numerical glazed PVT model developed in this work. The obtained results are in good agreement and the air outlet temperature values have a small difference with similar ambient conditions, mass flow rate and module area.

The numerical results obtained in the present study were also compared with results made by Slimani et al. [14]. For this validation, the thermo-physical properties are given in Fig. 7(a). The simulated values of the air outlet temperature and PV cell temperature are close to the corresponding results whereas PV cell efficiency closely aligns with a slight distinction, even under maximum solar radiation. On the other hand, the variation of air outlet temperature difference has been shown in Fig. 7(b) with different mass flow rates. It has been observed that the occurring difference between the two studies is less than 1 °C for the air outlet temperature. Airflow rate is an important parameter in a PVT system, one can observe that the increase in mass flow rate, reduces the air outlet temperature.

Furthermore, the values computed by the developed bi-fluid model are compared with the values reported in Bakar et al. [39], as shown in Table 2. By considering similar ambient conditions, the mean and outlet water temperatures presented in this study align closely with the outcomes observed in previous studies. Since two different fluids are

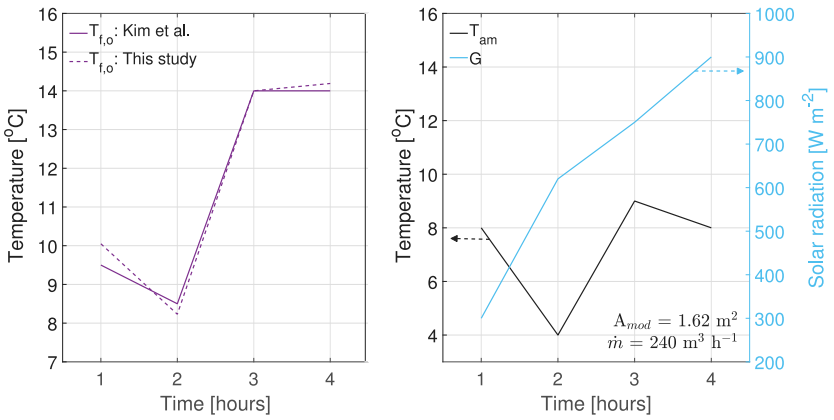

(a) Left - Evolution of air flow outlet temperature by Kim et al. (2014) and this study, Right - Solar radiation and ambient temperature input.

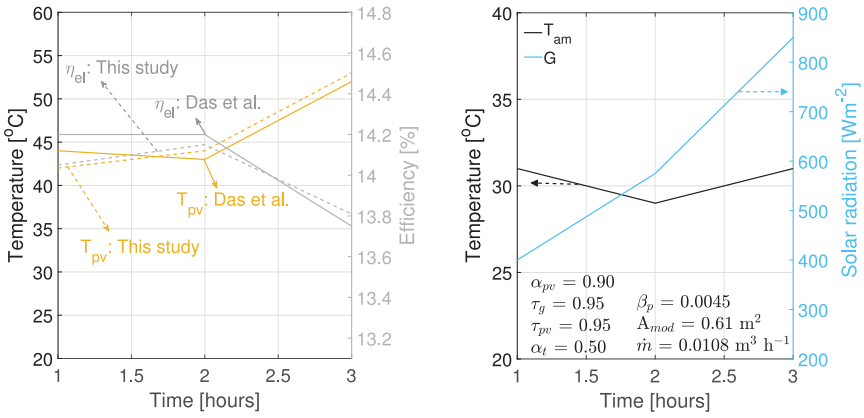

(b) Left - Evolution of PV cell temperature and PV efficiency by Das et al. (2017) and this study, Right - Solar radiation and ambient temperature input.

Fig. 5. Validation of unglazed PVT collector: a comparative analysis between this study and existing literature studies.

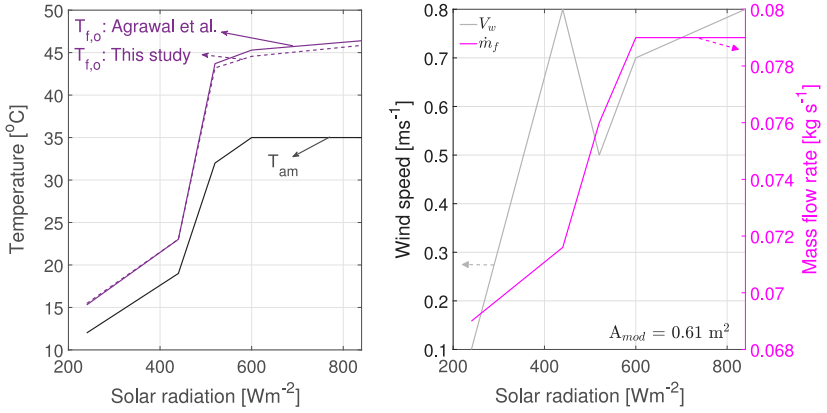

Fig. 6. Validation of glazed PVT collector: Left — evolution of ambient temperature, air flow outlet temperature by Agrawal and Tiwari [49] and this study, Right — Wind speed and mass flow rate input.

used in this type of collector, the instantaneous thermal efficiency (air) is also compared. It can be observed in Table 3 that with the variation in mass flow rate, the resultant efficiency is related to the values obtained in previous studies and both fluids results are in good agreement.

In general, the simulation results founded by the numerical PVT models developed in this study and other studies in the literature validate the viability and accuracy of the presented models.

4.2. PVT collectors

The hourly evolution of ambient temperature for three days in Amsterdam region with different solar irradiance is compared in Fig. 8. The maximum solar radiation observed during the first day is just above 800 Wm^{-2} and the corresponding ambient temperature is 25.30 °C, around solar noon. In all the investigated configurations, similar

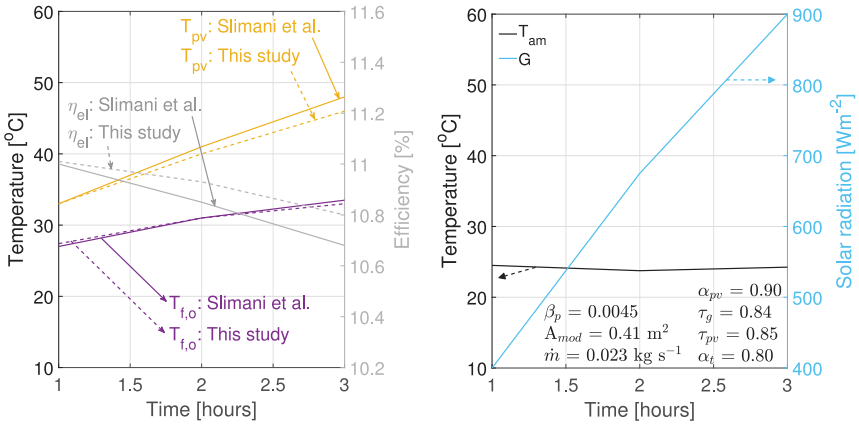

(a) Left - Evolution of PV cell, air flow outlet temperatures and PV efficiency by Slimani et al. (2017) and this study, Right - Solar radiation and ambient temperature input.

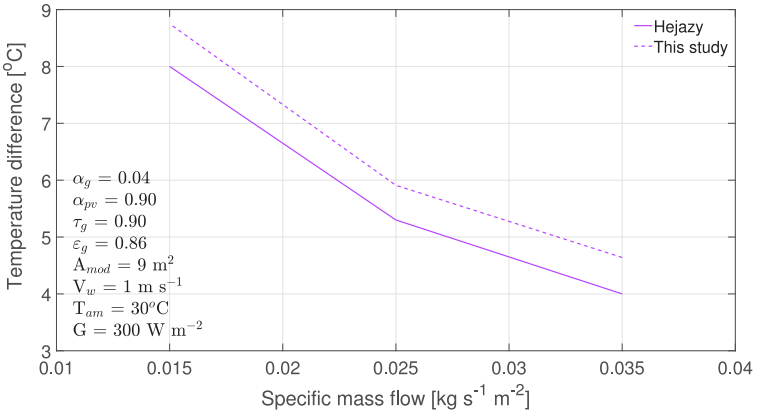

(b) Evolution of temperature difference by Hegazy (2000) and this study.

Fig. 7. Validation of dual channel PVT collector: a comparative analysis between this study and existing literature studies.

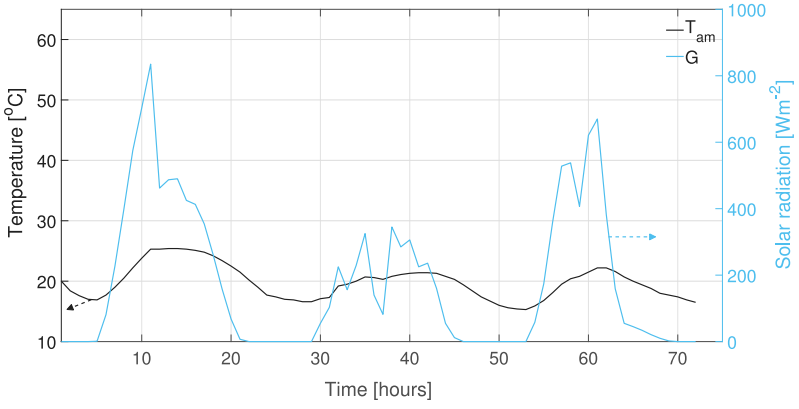

Fig. 8. The hourly evolution of solar radiation and ambient temperature in Amsterdam region.

Table 3
Validation of a bi-fluid PVT collector — air part: a comparison between this study and study done by [39].

$\dot{m}_f$	η_f [%]	
	[39]	This study
0.04	26	25
0.08	29	29

wind speed and mass flow rate profiles were used and the air inlet temperature is assumed to be equal to the ambient temperature.

The air inlet temperature to the air-based PVT collectors at $L = 0$ is taken equal to the ambient temperature, such that $T_{f,in} = T_{am}$, i.e. no air recycling. Fig. 9 presents an hourly comparison of PV cell components and air outlet temperatures for the three air-based PVT configurations. Dual channel configuration utilizes more area, making it the best fluid heating option. On the other hand, the unglazed type PVT configuration has the best PV cooling. The temperatures of the PV module components reach their peak over the course of three days and the use of extra glass (glazed configuration) leads to a higher and more effective thermal output. However the PV cell temperature

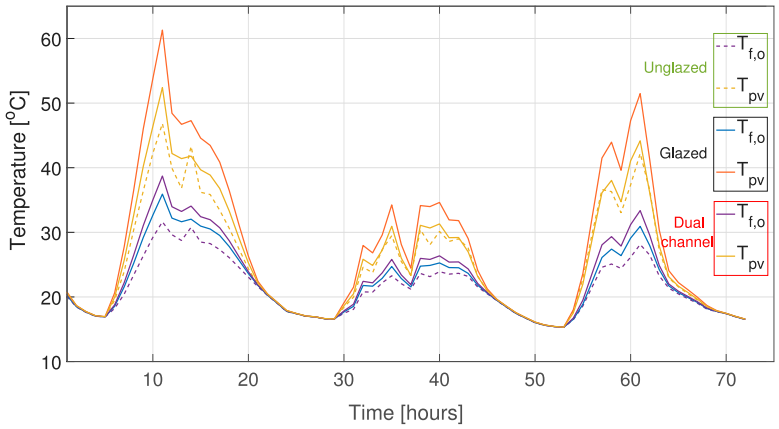

Fig. 9. The hourly comparison of PV cell and air outlet temperatures in unglazed (green), glazed (black) and dual channel (red) air-based PVT collectors in Amsterdam region. (For interpretation of the references to color in this figure legend, the reader is referred to the web version of this article.)

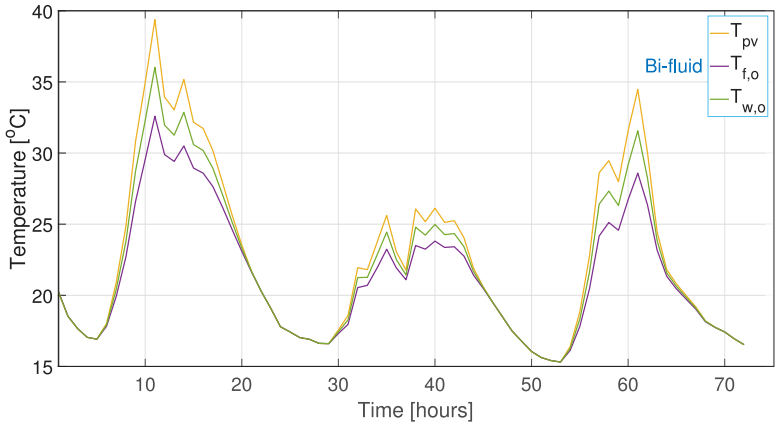

Fig. 10. The hourly evolution of PV cell and fluids outlet temperatures in a bi-fluid PVT collector in Amsterdam region.

reaches a maximum value of around 60 °C compared to 46.80 °C for unglazed PVT configuration, consequently, this leads to a decrease in PV performance. For the PV and thermal energy output calculation, the solar irradiance, ambient temperature, wind speed and non-linearity responses are taken into consideration.

Fig. 10 illustrates the hourly evolution of PV cell and fluids outlet temperatures in a bi-fluid PVT configuration. Here, water and air circulate simultaneously through the collector, extracting the maximum amount of waste heat. This maximum extraction of heat lowers the PV module temperature which ultimately results in a higher PV efficiency. The mass flow rates considered for the two fluids (water and air) are 0.015 and 0.01 kgs^{-1}. In contrast to configurations relying solely on air, the temperature of PV cells is lower due to the presence of two heat extraction mediums circulating beneath the PV module. At solar radiation of above 800 Wm^{-2}, the PV cell temperature rises to 40 °C whereas the water outlet temperature can go above 35 °C with outdoor temperature serving as the inlet temperature. Taking into account the inlet and outlet temperatures, the thermal efficiency for water reaches 45%, whereas the thermal efficiency of air attains a value of 10%.

The hourly evolution of glazed PVT component temperatures is illustrated in Fig. 11. The observed temperatures in this setup are the temperatures of PV module components (glass, confined air space, cell, tedlar), insulator and outlet air temperature. It can be observed that the PV cell layer has the highest temperature and all collector component temperatures are higher than the ambient temperature. The addition of a glass cover above the PV module leads to an increase in the temperature of all collector components. The outlet air temperature reaches to 37.30 °C at this point with the mass flow rate of 0.01 kgs^{-1}, which means that the difference between the inlet air temperature and the outlet air temperature can reach 12 °C with this ambient conditions. This is because the fluid circulating below the PV module is air which has lower heat transfer than water, phase change material (PCM), or some other fluids (i.e. nano-fluids).

As the data is collected, the comparison of the thermal efficiency obtained from different air-based configurations and the total thermal efficiency curve for bi-fluid configuration is compared in Fig. 12, demonstrating thermal performance characteristics as a function of operation conditions $(T_{in} - T_{am})/G$. It is obvious that for the bi-fluid configuration, the slope of the thermal efficiency curve is high in comparison to the air-based configurations. It is interesting that the efficiency curve for unglazed type configuration exhibits a more rapid reduction when contrasted with glazed type configuration.

The monthly solar radiation profile (Fig. 13) for the Amsterdam region reveals solar energy availability throughout the year. The profile exhibits seasonal changes, with higher solar radiation levels during the summer months and relatively lower levels during the winter months. Furthermore, the average monthly ambient temperature profile is illustrated, showcasing the typical temperature variations throughout the year, indicating colder temperatures during the winter months, with January and December being the coldest. As the year progresses, the temperature gradually rises, reaching its peak during the summer

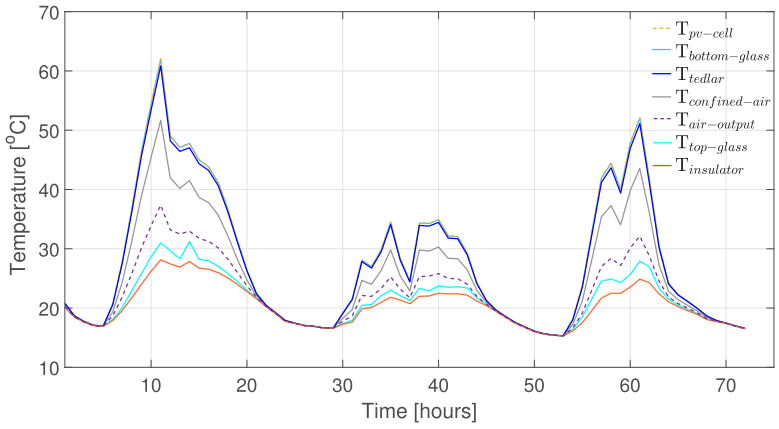

Fig. 11. The hourly evolution of temperature components in glazed air-based PVT collector in Amsterdam region.

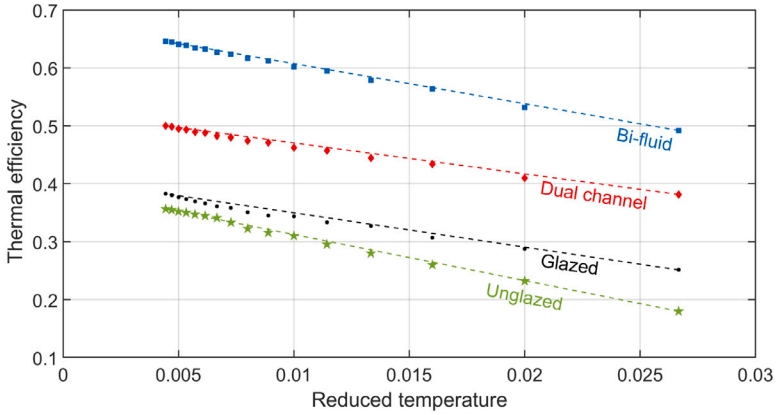

Fig. 12. Thermal efficiency curve of unglazed, glazed, dual channel and bifluid collectors as a function of operation condition.

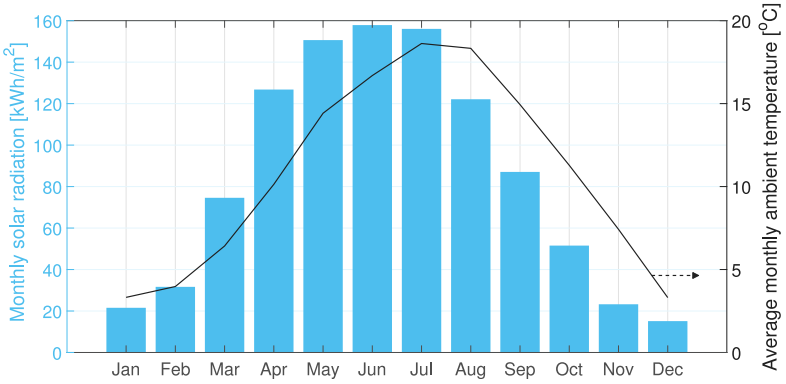

Fig. 13. Monthly solar radiation and average ambient temperature in Amsterdam region.

months, particularly in July. The seasonal cycle is clearly visible when looking at the average monthly ambient temperature.

The monthly electrical and thermal energy production is comprehensively compared for all four PVT configurations, throughout the year in Fig. 14. During the colder months, particularly in winter, the power production is lower in contrast to warmer months. During May, June and July, the peak months, all configurations produce the most energy output. The significant increase is attributed to the high irradiation and an abundance of sun hours. Among all the four configurations, the bi-fluid configuration produces the highest annual thermal and electrical outputs whereas the unglazed configuration demonstrates the lowest thermal output (≈ 225 kWhm^{-2}). On the other hand, the glazed configuration exhibits the lowest annual electrical output (≈ 131 kWhm^{-2}) among all the four setups.

These results are then used to calculate the annual thermal and electrical outputs of the system, with the final aim of obtaining the APE. In Fig. 15, a comparison of the APE achievable per square meter using various PVT configurations is presented. For the unglazed configuration, the APE stands at approximately 682 kWhm^{-2} per year, while for the bi-fluid configuration, it is around 1183 kWhm^{-2} per year, the highest among all the four configurations. On the other hand, the glazed type and dual channel exhibit an APE of approximately 814 and 930 kWhm^{-2} per year. This comparison demonstrates the immense potential of PVT systems in harnessing both electrical and thermal

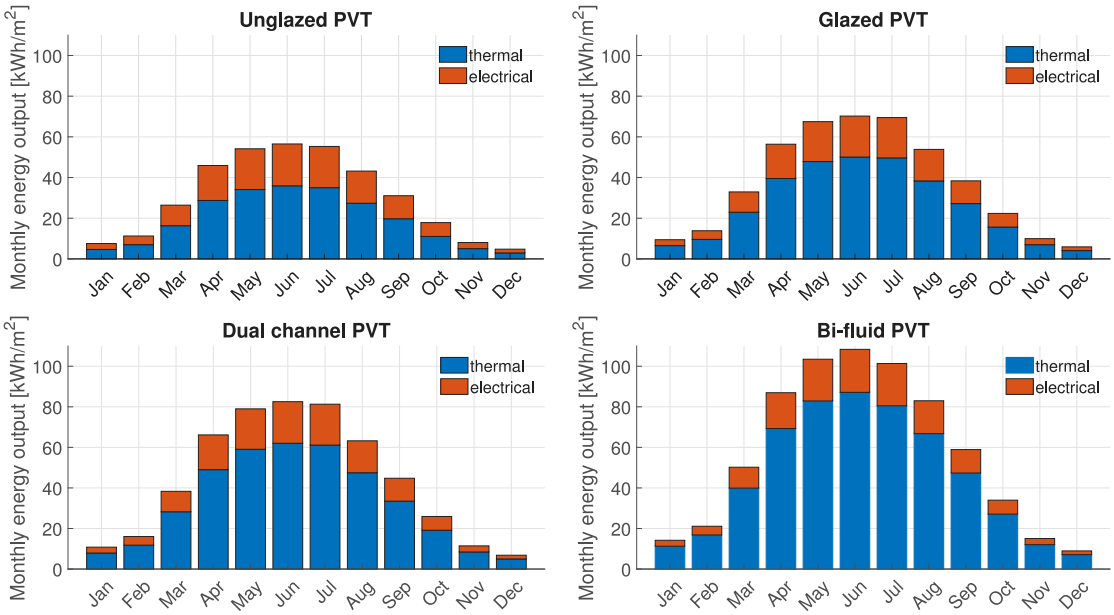

Fig. 14. Monthly prediction of thermal and electrical energy outputs for Amsterdam region.

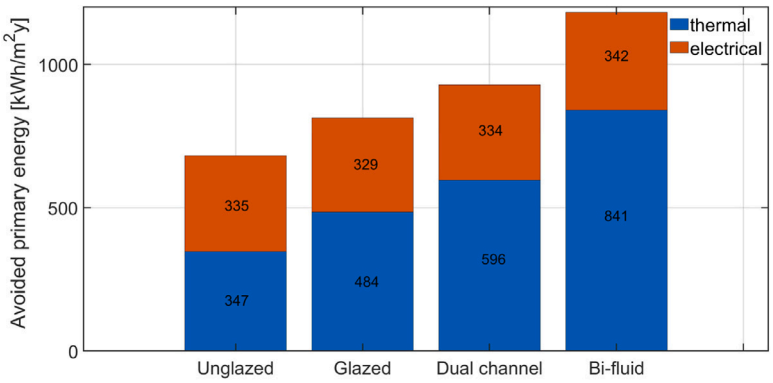

Fig. 15. A comparison of avoided primary energy (APE) per m^2 of the PVT collectors in Amsterdam region.

energy concurrently, making them a compelling and sustainable choice for energy generation and conservation.

In addition, six different cities (Beijing (EM), China; Amsterdam (DL), Netherlands; Lahore (CH), Pakistan; Manila (AH), Philippines; Phoenix (BK), USA and Tangier (DH), Morocco) from the northern hemisphere were targeted to compare the heat and power production, each city representing a distinct KGPV zone. The initial letter denotes the temperature-precipitation (TP)-zones: A-Tropical, B-Desert, C-Steppe, D-Temperate, E-Cold and F-Polar. The second letter denotes the Irradiation (I)-zones: K-Very High, H-High, M-Medium and L-Low irradiation. Since large PV or PVT systems are usually installed in or next to populated areas, this is why these cities were selected, while the overlooked zones can be likened to their closest neighboring zone for comparison. The annual electrical output, thermal output and APE for each city were calculated for the different PVT configurations as shown in Fig. 16. In addition, it provides the annual solar radiation data for all six cities. This study showed that Phoenix Desert, USA produced the highest annual output because of very high irradiation and high numbers of sun hours. However, high PV cell temperatures can be harmful to the performance of the collectors. In terms of average PV module efficiency, the highest efficiency observed was for the Beijing, China (unglazed: 13.15%, glazed: 12.85%, dual-channel: 13.00% and bi-fluid: 13.50%, respectively) because of medium solar radiation, surpassing cities such as Phoenix (unglazed: 12.50%, glazed: 12.00%, dual-channel: 12.20% and bi-fluid: 13.00%, respectively), and Tangier (unglazed: 12.95%, glazed: 12.50%, dual-channel: 12.70% and bi-fluid: 13.45%, respectively), which experience very high irradiation. The annual thermal energy production is lower due to the lower ambient temperature and irradiation levels. Moreover, the thermal output of the bi-fluid based PVT collectors is very high compared to the other three air-based configurations. This is due to the fact that two different fluids circulate simultaneously below the PV module and extract most of the waste heat. The use of water in this configuration is more effective at transferring heat than using only air as a heat extraction medium. Additionally, it was observed that the use of bi-fluids in the PVTs results in enhanced PV module performance. Lastly, the time step chosen for these collectors is 1 s. Nevertheless, considering that the PVMD toolbox [28] operates on hourly-based data, employing a time step of 1 h suffices for accurate calculations in capturing the dynamics of system.

4.3. Novel bi-fluid PVT system

In Section 4.2, results for only bifluid PVT collector are presented for the Amsterdam region. However, for the novel bi-fluid PVT system, the collector is integrated with a storage tank, controller and auxiliary heaters. For this study, the DHW consumption profiles [18,50] used are

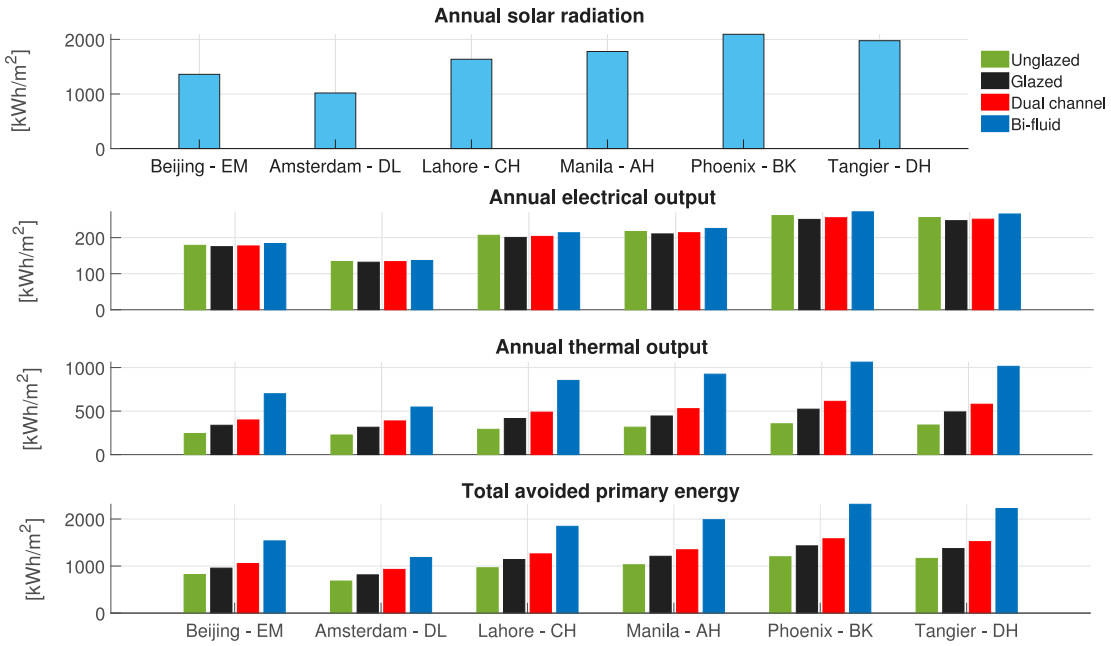

Fig. 16. A comparison of electrical output ($\mathscr{P}_{el}$), thermal output ($\mathscr{P}_{th}$) and avoided primary energy (APE) of the PVT collectors and annual solar radiation according to locations.

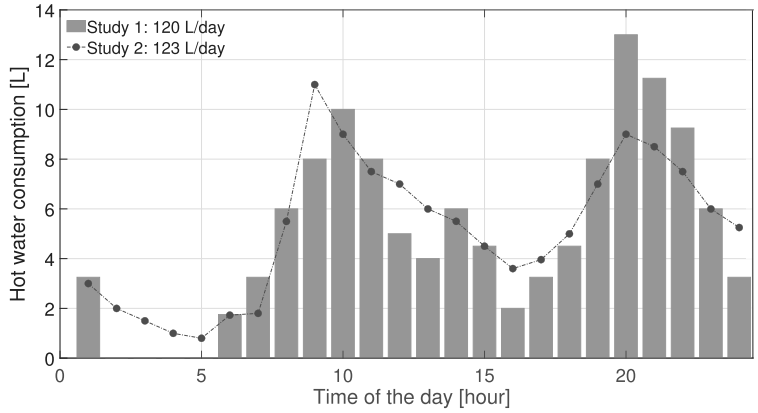

Fig. 17. Domestic hot water daily consumption profile [18,50].

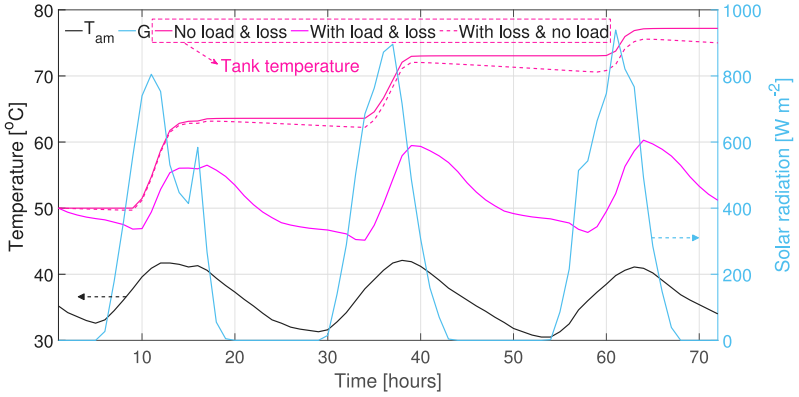

Fig. 18. Storage tank temperature integrated with a bi-fluid collector for domestic hot water in Lahore. The top line signifies no load and no loss, the middle illustrates loss with no load, while the bottom denotes operation under load with loss.

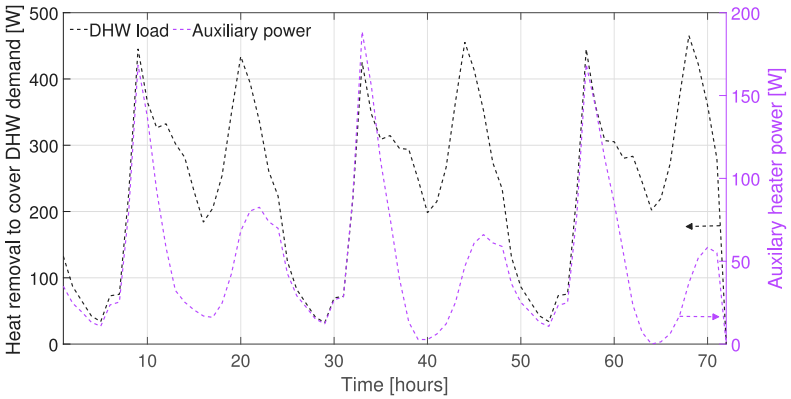

Fig. 19. Hourly load and auxiliary power required for domestic hot water in Lahore.

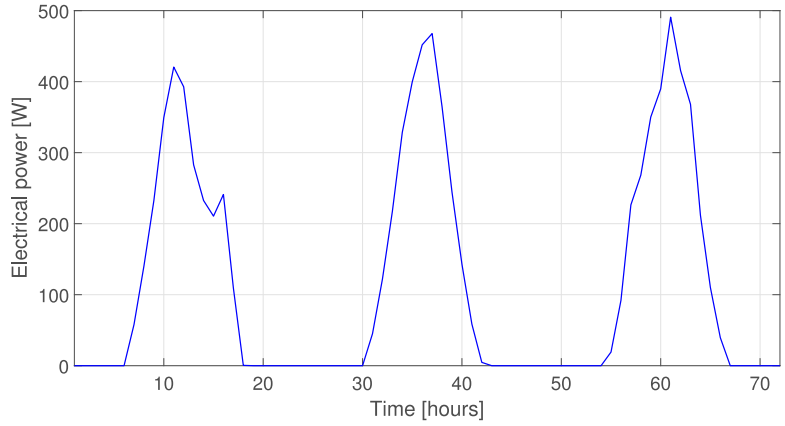

Fig. 20. Generated electrical power by bi-fluid PV module in Lahore.

depicted in Fig. 17 considering UK and Cyprus-based studies. These calculations are based on an assumed daily consumption of approximately 120 liters of hot water at 60 °C, customized for a family comprising four individuals (equivalent to 30 liters per person). Sustained demand for DHW persists throughout the year without too much variation.

Fig. 18 shows results from the 20th to the 22nd of June for Lahore city in Pakistan. The temperature of the hot-water storage tank increases considerably without any load, no water is extracted from the tank. However, the tank temperature drops slightly because of the heat losses through the walls of the tank. This happens when a family goes on a two-day vacation (weekend) and makes it possible to cover a higher amount of DHW demand on the following day. By extracting hot water from the tank (mean household hot water consumption is approximately 120 Liters/day for 120 m^2 house based on a four-member family) and considering heat losses through the walls, the tank temperature is close to or above 60 °C during main hours of the day.

The energy removal to supply the DHW demand is illustrated in Fig. 19. However, auxiliary heat becomes necessary to increase the tank temperature, particularly during the early morning and late evening hours to supply the hot water at 60 °C to the house. It is important to note that the initial temperature of the tank is assumed close to the temperature final temperature. The water temperature for tank filling was precisely set to 12 °C.

The efficacy and feasibility of the PVT system design depends significantly on the electrical power output which is directly influenced by solar irradiance, PV cell temperature and fluid mass flow rate. Fig. 20 illustrates the hourly fluctuations in generated electric power over the course of three days. The total electrical yield in the given period is approximately 1.60 $kWhm^{-2}$.

The DHW heating load, encompassing both solar and auxiliary sources, is illustrated in Fig. 21. Analysis reveals that the heating demand peaks during colder months, demonstrating a discernible seasonal variation. Conversely, during the summer months, the load decreases slightly, reflecting a seasonal modulation in the energy requirements for DHW. Further, the fraction of thermal energy demand covered by the system is shown on the right axis. The fraction of energy covered demonstrates a notable increase throughout the summer months, due to higher solar irradiance levels. The system can cover above 30% of the total demand of DHW during the peak winter months. On the other hand, the system can cover between 65% to 80% of DHW demand for the rest of the months. With the gross bi-fluid collector surface area of 4.33 m^2, a 200 L storage tank, can cover more than 59% annual DHW demand in Lahore.

Note that more heat could be generated if a larger surface area of the PVT collector is used however as the collector area gets bigger, the thermal efficiency decreases. For example, the cities like the Amsterdam and Beijing have low and medium annual solar radiation (1018 and 1360 $kWhm^{-2}$, respectively), only 32% and 39% of the total DHW demand over a year can be covered by said system. Given the lack of solar radiation, it is reasonable to employ more collectors to cover the demand. At the same time, cities like Manila and Phoenix have high annual solar radiation (1778 and 2094 $kWhm^{-2}$, respectively). The system is well-suited for small houses, as it effectively covers 63% to 70% of the total DHW demand over the course of a year, where DHW consumption shows minimal variation throughout the year.

The Fig. 22 illustrates the external factors, namely ambient temperature, solar radiation, and wind speed, which are exerted upon the system. These external variables have a significant impact on the

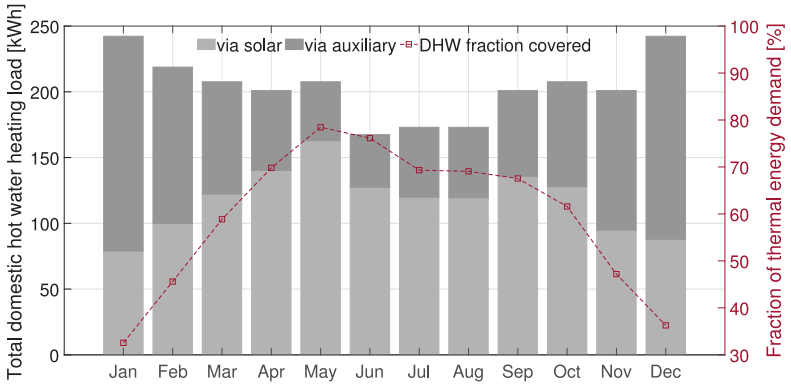

Fig. 21. Monthly fraction of thermal energy demand covered for domestic hot water in Lahore.

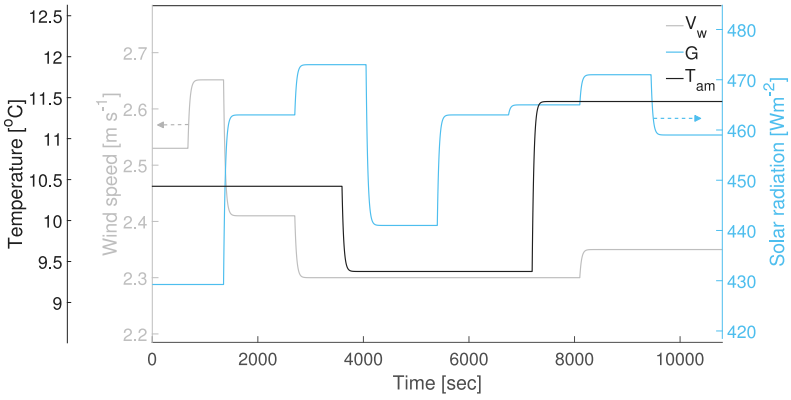

Fig. 22. External disturbances imposed on the novel bi-fluid PVT system.

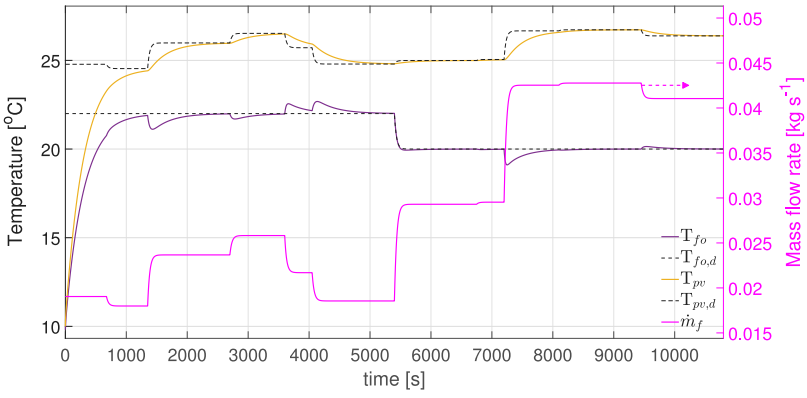

Fig. 23. Tracking of desired outlet air temperature, reference setpoint by PV cell state variable and control input exerted on the system.

collector's outlet air temperature and are randomly chosen. Notably, an increase in wind speed led to a decrease in output, while the ambient temperature and solar radiation exhibited an opposite effect. It is noteworthy that throughout these fluctuations, the system maintained effective tracking of the setpoint. For SH as shown in Fig. 23, the controller tracks the desired temperature setpoints of 22 °C and 20 °C even with the fluctuations in external factors. Steady-state error was negligible, measuring less than 0.10 °C, demonstrating the controller's precision in tracking the setpoint. The controller turned on, only when heating is required and it works within a certain range of ambient temperature which is taken as fluid inlet temperature to the collector. Thus, if the ambient temperature or the solar irradiation go very low, the auxiliary heater is utilized as air has low heat transfer. The temperature of PV cell is also illustrated as it is an important parameter and directly influences the PV power. The control input played a pivotal role in regulating the air outlet temperature of the system. By manipulating the mass flow rate, the controller effectively adjusted the desired temperature required for SH and is shown in Fig. 23. It can also be observed that increasing the mass flow rate resulted in a lower air outlet temperature, while decreasing it led to a high temperature.

5. Conclusions

The present effort focuses on the performance of air-based PVT collectors and a novel multi-functional bi-fluid based PVT system integrated with a storage tank and a controller for domestic hot water, space heating and generating electrical power for a single residential house. The main findings of this study are summarized as follow:

- In Amsterdam region, the unglazed configuration emerges as the optimal choice for efficient PV cooling among air-based collectors (≈ 134 $kWhm^{-2}$), effectively maximizing PV energy output. Conversely, the dual-channel configuration excels in its capacity for air heating, offering unparalleled performance in harnessing thermal energy (≈ 546 $kWhm^{-2}$). Moreover, the bi-fluid PVT collector emerges as the top performer in electricity generation. This is attributed to its unique feature of simultaneous circulation of two fluids, which effectively maintains lower cell temperatures.
- Utilization of two different fluids combines the advantages and this combination not only enhances thermal output but also effectively reduces the PV cell temperature.
- When it comes to APE, a bi-fluid collector shows the biggest energy savings per m^2 (≈ 1183 $kWhm^{-2}$ per year), while an unglazed collector exhibits the smallest (≈ 682 $kWhm^{-2}$ per year) in Amsterdam region.
- Given the specific collector area and locations analyzed in this study, the extent to which the annual thermal energy demand for domestic hot water is met varies, ranging from 32% to 70%. This variability is directly influenced by the annual solar radiation and ambient temperature at each location.
- On the other hand, it has been shown that the use of a robust control approach not only tracks the desired set points but also rejects the external disturbances and variations imposed on the system.

The preparation for testing is underway, and the experiment will take place in the future. Here are some ways we can enhance the current findings in the future:

- During the summer season, a combination of auxiliary heater and hot water stored in a domestic storage tank can be used to generate cooling energy in thermally-driven cooling options.
- In regions characterized by low irradiance levels and consistently low ambient temperatures necessitating year-round SH, consider the economical choice of integrating air-based PVT collectors with a heat pump or auxiliary heater.
- The utilization of an aquifer thermal energy storage (ATES) system is a smart choice for storing energy across seasons.
- The superiority of water-based over air-based collector is obvious as water has better heat transfer properties. Consequently, a comparison between bi-fluid and water-based collector considering different configurations and flow passages would be interesting.

Taking all the results into consideration, it can be concluded that PVT systems possess a significant potential for effectively decarbonizing urban areas. However, it is important to note that the commercialization and practical usability of PVT modules remain limited.

CRediT authorship contribution statement

Zain Ul-Abdin: Conceptualization, Data curation, Methodology, Validation, Writing – original draft, Writing — review & editing. **Miro Zeman:** Funding acquisition. **Olindo Isabella:** Funding acquisition, Project administration, Writing – review & editing. **Rudi Santbergen:** Conceptualization, Methodology, Supervision, Writing – review & editing.

Declaration of competing interest

The authors declare that they have no known competing financial interests or personal relationships that could have appeared to influence the work reported in this paper.

Acknowledgments

This project has been developed in the framework of the PED Program, which is implemented by the Joint Programming Initiative Urban Europe and SET Plan Action 3.2. The Austrian part is supported by the Austrian Ministry of Climate Action, Environment, Energy, Mobility, Innovation, and Technology (BMK); the Romanian part is supported by a grant of the Ministry of Research, Innovation and Digitization CNCS/CCCDI – UEFISCDI, Romania, project number PED-JPI-SIMPLY POSITIVE, contracts number 325/2022 and 326/2022, within PNCDI III; the Dutch part is supported by the RVO, The Netherlands (the Netherlands Enterprise Agency), reference number ERANETPED-02767306; and the Italian part is supported by a grant of the Ministry of Education and Merit - Department for Higher Education and Research, Italy, project number PED_00042, from the Fund for Investment in Scientific and Technological Research (FIRST/FAR) and/or Special Accounting Account no. 5944.

References

[1] REN21, Renewables 2023 global status report collection, renewables in energy supply, Technical report, 2023.
[2] M. Herrando, K. Wang, G. Huang, T. Otanicar, O.B. Mousa, R.A. Agathokleous, Y. Ding, S. Kalogirou, N. Ekins-Daukes, R.A. Taylor, et al., A review of solar hybrid photovoltaic-thermal (pv-t) collectors and systems, Prog. Energy Combust. Sci. 97 (2023) 101072.
[3] L.W. Thong, S. Murugan, P.K. Ng, C.C. Sun, Analysis of photovoltaic panel temperature effects on its efficiency, System 18 (19) (2016).
[4] P.M.J. Stalin, K.S. Prasad, K.P. Kumar, G. Hemadri, M. Rajesh, K.P. Kumar, Performance improvement of solar pv through the thermal management using a nano-pcm, Mater. Today: Proc. 50 (2022) 1553–1558.
[5] Z. Ul Abdin, A. Rachid, A survey on applications of hybrid pv/t panels, Energies 14 (4) (2021) 1205.
[6] A.M. Alshibil, I. Farkas, P. Víg, Multi-aspect approach of electrical and thermal performance evaluation for hybrid photovoltaic/thermal solar collector using trnsys tool, Int. J. Thermofluids 16 (2022) 100222.
[7] B. Widyolar, L. Jiang, J. Brinkley, S.K. Hota, J. Ferry, G. Diaz, R. Winston, Experimental performance of an ultra-low-cost solar photovoltaic-thermal (pvt) collector using aluminum minichannels and nonimaging optics, Appl. Energy 268 (2020) 114894.
[8] M.A. Hasan, K. Sumathy, Photovoltaic thermal module concepts and their performance analysis: a review, Renew. Sustain. Energy Rev. 14 (7) (2010) 1845–1859.
[9] V. Tyagi, S. Kaushik, S. Tyagi, Advancement in solar photovoltaic/thermal (pv/t) hybrid collector technology, Renew. Sustain. Energy Rev. 16 (3) (2012) 1383–1398.
[10] R. Daghigh, M.H. Ruslan, K. Sopian, Advances in liquid based photovoltaic/thermal (pv/t) collectors, Renew. Sustain. Energy Rev. 15 (8) (2011) 4156–4170.
[11] A. Rachid, A. Goren, V. Becerra, J. Radulovic, S. Khanna, Solar pvt systems, in: Solar Energy Engineering and Applications, Springer, 2022, pp. 83–104.
[12] R. Santbergen, C. Rindt, H. Zondag, R.C. Van Zolingen, Detailed analysis of the energy yield of systems with covered sheet-and-tube pvt collectors, Sol. Energy 84 (5) (2010) 867–878.
[13] A.A. Hegazy, Comparative study of the performances of four photovoltaic/thermal solar air collectors, Energy Convers. Manag. 41 (8) (2000) 861–881.
[14] M.E.A. Slimani, M. Amirat, I. Kurucz, S. Bahria, A. Hamidat, W.B. Chaouch, A detailed thermal-electrical model of three photovoltaic/thermal (pv/t) hybrid air collectors and photovoltaic (pv) module: Comparative study under algiers climatic conditions, Energy Convers. Manag. 133 (2017) 458–476.
[15] S. Agrawal, G. Tiwari, Overall energy, exergy and carbon credit analysis by different type of hybrid photovoltaic thermal air collectors, Energy Convers. Manag. 65 (2013) 628–636.
[16] J. Ma, W. Sun, J. Ji, Y. Zhang, A. Zhang, W. Fan, Experimental and theoretical study of the efficiency of a dual-function solar collector, Appl. Therm. Eng. 31 (10) (2011) 1751–1756.

[17] J. Ji, C. Guo, W. Sun, W. He, Y. Wang, G. Li, Experimental investigation of tri-functional photovoltaic/thermal solar collector, Energy Convers. Manag. 88 (2014) 650–656.
[18] I. Guarracino, A. Mellor, N.J. Ekins-Daukes, C.N. Markides, Dynamic coupled thermal-and-electrical modelling of sheet-and-tube hybrid photovoltaic/thermal (pvt) collectors, Appl. Therm. Eng. 101 (2016) 778–795.
[19] K.M. Powell, T.F. Edgar, Modeling and control of a solar thermal power plant with thermal energy storage, Chem. Eng. Sci. 71 (2012) 138–145.
[20] E. Bellos, C. Tzivanidis, K. Moschos, K.A. Antonopoulos, Energetic and financial evaluation of solar assisted heat pump space heating systems, Energy Convers. Manag. 120 (2016) 306–319.
[21] Z. Ul Abdin, A. Rachid, Modeling, identification and control of photovoltaic/thermal solar panel, in: 2020 IEEE Conference on Control Technology and Applications, CCTA, IEEE, 2020, pp. 1–6.
[22] M. Zamen, A. Baghban, S.M. Pourkiaei, M.H. Ahmadi, Optimization methods using artificial intelligence algorithms to estimate thermal efficiency of pv/t system, Energy Sci. Eng. 7 (3) (2019) 821–834.
[23] H. Ravaee, S. Farahat, F. Sarhaddi, Artificial neural network based model of photovoltaic thermal (pv/t) collector, J. Math. Comput. Sci. 4 (3) (2012) 411–417.
[24] I. Guarracino, J. Freeman, A. Ramos, S.A. Kalogirou, N.J. Ekins-Daukes, C.N. Markides, Systematic testing of hybrid pv-thermal (pvt) solar collectors in steady-state and dynamic outdoor conditions, Appl. Energy 240 (2019) 1014–1030.
[25] J. Chen, L. Zhang, Y. Dai, Performance analysis and multi-objective optimization of a hybrid photovoltaic/thermal collector for domestic hot water application, Energy 143 (2018) 500–516.
[26] N. Aste, C. Del Pero, F. Leonforte, Water pvt collectors performance comparison, Energy Procedia 105 (2017) 961–966.
[27] A. Ibrahim, M.Y. Othman, M.H. Ruslan, M. Alghoul, M. Yahya, A. Zaharim, K. Sopian, Performance of photovoltaic thermal collector (pvt) with different absorbers design, Wseas Trans. Environ. Dev. 5 (3) (2009) 321–330.
[28] M. Vogt, C.R. Tobon, A. Alcaniz, P. Procel, Y. Blom, A.N. El Din, T. Stark, Z. Wang, E.G. Goma, J. Etxebarria, et al., Introducing a comprehensive physics-based modelling framework for tandem and other pv systems, Sol. Energy Mater. Sol. Cells 247 (2022) 111944.
[29] Y. Agrawal, A. Mishra, A. Gautam, G. Phaldessai, A.S. Yadav, M. Vyas, Performance analysis of photovoltaic thermal air collector having rectangular fins, Mater. Today: Proc. 84 (2023) 6–15.
[30] S. Algarni, D. Nutter, Survey of sky effective temperature models applicable to building envelope radiant heat transfer, Ashrae Trans. 121 (2) (2015).
[31] Z. Ul Abdin, Modeling and control of hybrid PV thermal panels, (Ph.D. thesis), Université de Picardie Jules Verne, 2022.
[32] M. Ahmadinejad, R. Moosavi, Energy and exergy evaluation of a baffled-nanofluid-based photovoltaic thermal system (pvt), Int. J. Heat Mass Transfer 203 (2023) 123775.
[33] S. Alsaqoor, A. Alqatamin, A. Alahmer, Z. Nan, Y. Al-Husban, H. Jouhara, The impact of phase change material on photovoltaic thermal (pvt) systems: A numerical study, Int. J. Thermofluids 18 (2023) 100365.
[34] H.P. Singh, A. Jain, A. Singh, S. Arora, Influence of absorber plate shape factor and mass flow rate on the performance of the pvt system, Appl. Therm. Eng. 156 (2019) 692–701.
[35] H. Vajedi, M. Dehghan, M. Aminy, A. Pourrajabian, G.G. Ilis, Experimental study on an air-based photovoltaic-thermal (pv-t) system with a converging thermal collector geometry: a comparative performance analysis, Sustain. Energy Technol. Assess. 52 (2022) 102153.
[36] M. Hissouf, M. Najim, A. Charef, et al., Numerical study of a covered photovoltaic-thermal collector (pvt) enhancement using nanofluids, Sol. Energy 199 (2020) 115–127.
[37] K. Hollands, T. Unny, G. Raithby, L. Konicek, Free convective heat transfer across inclined air layers, 1976.
[38] Y. Yu, E. Long, X. Chen, H. Yang, Testing and modelling an unglazed photovoltaic thermal collector for application in sichuan basin, Appl. Energy 242 (2019) 931–941.
[39] M.N.A. Bakar, M. Othman, M.H. Din, N.A. Manaf, H. Jarimi, Design concept and mathematical model of a bi-fluid photovoltaic/thermal (pv/t) solar collector, Renew. Energy 67 (2014) 153–164.
[40] A. Esser, F. Sensfuss, C. Amann, Final report evaluation of primary energy factor calculation options for electricity, Fraunhofer-Institut für System-und Innovationsforschung (ISI) (2016).
[41] M. Herrando, C.N. Markides, K. Hellgardt, A uk-based assessment of hybrid pv and solar-thermal systems for domestic heating and power: System performance, Appl. Energy 122 (2014) 288–309.
[42] G. Rigatos, Nonlinear optimal control for the multi-variable tumor-growth dynamics, Comput. Methods Biomech. Biomed. Eng. (2023) 1–29.
[43] R. Lazzarin, Heat pumps and solar energy: A review with some insights in the future, Int. J. Refrig. 116 (2020) 146–160.
[44] Y. Zhang, J. Ji, Z. Song, W. Ke, H. Xie, Performance prediction on a novel dual-mode heat pump with a hybrid photovoltaic/micro-channel heat pipe/fin heat exchanger, Energy Convers. Manage. 293 (2023) 117505.
[45] R. Yumrutaş, M. Ünsal, Energy analysis and modeling of a solar assisted house heating system with a heat pump and an underground energy storage tank, Sol. Energy 86 (3) (2012) 983–993.
[46] S.A. Kalogirou, Solar Energy Engineering: Processes and Systems, Academic Press, 2013.
[47] J.-H. Kim, S.-H. Park, J.-T. Kim, Experimental performance of a photovoltaic-thermal air collector, Energy Procedia 48 (2014) 888–894.
[48] B. Das, B. Rezaie, P. Jha, R. Gupta, Performance analysis of single glazed solar pvt air collector in the climatic condition of ne india, in: Proceedings, Vol. 2, MDPI, 2017.
[49] S. Agrawal, G. Tiwari, Exergoeconomic analysis of glazed hybrid photovoltaic thermal module air collector, Sol. Energy 86 (9) (2012) 2826–2838.
[50] S.A. Kalogirou, Use of trnsys for modelling and simulation of a hybrid pv–thermal solar system for cyprus, Renew. Energy 23 (2) (2001) 247–260.